

# **CELLULAR ROLES OF GLUTAMATE TRANSPORTER-ASSOCIATED ANION CHANNELS IN GLIAL CELLS**

Inaugural-Dissertation

zur Erlangung des Doktorgrades  
der Mathematisch-Naturwissenschaftlichen Fakultät  
der Heinrich-Heine-Universität Düsseldorf

vorgelegt von

**Verena Untiet**  
aus Seligenstadt

Jülich, Dezember 2015

aus dem Institute of Complex Systems – Zelluläre Biophysik  
des Forschungszentrums Jülich

Gedruckt mit der Genehmigung der  
Mathematisch-Naturwissenschaftlichen Fakultät der  
Heinrich-Heine-Universität Düsseldorf

Referent: Prof. Dr. Christoph Fahlke

Korreferent: Prof. Dr. Christine R. Rose

Tag der mündlichen Prüfung: 02. Dezember 2016

Für Lina Christine Elfriede Hilge



# Contents

List of figures .....	IV
List of tables .....	VI
1 Abstract .....	1
2 Zusammenfassung.....	2
3 Introduction.....	3
3.1 Excitatory amino acid transporters (EAATs).....	3
3.2 The role of glial isoforms of EAATs in diseases.....	5
3.2.1 Altered EAAT1/GLAST anion conduction is associated with episodic ataxia and epilepsy .....	5
3.2.2 The loss of glial EAAT2/GLT1 leads to lethal spontaneous seizures in mice .....	5
3.3 Working hypothesis .....	6
3.4 The cerebellum is the predominant expression side of EAAT1/GLAST.....	7
3.4.1 Cerebellar morphology .....	7
3.4.2 Cerebellar signalling circuit.....	8
3.5 Chloride homeostasis of Bergmann glia.....	8
3.5.1 Chloride accumulation in Bergmann glia .....	9
3.5.2 Anion channels in Bergmann glia.....	9
3.6 Chloride imaging.....	10
3.6.1 Fluorescence lifetime imaging microscopy.....	10
3.6.2 Measuring fluorescence lifetimes using time correlated single photon counting.....	12
3.6.3 The chloride sensitive fluorescent dye MQAE.....	12
3.6.4 Two photon microscopy .....	13
4 Materials & Methods .....	15

4.1 Chemicals and materials.....	15
4.2 Cell culture.....	15
4.2.1 Primary cultured astrocytes (pc-astrocytes).....	15
4.3 Animals .....	16
4.3.1 Mice maintenance .....	16
4.3.2 EAAT1/GLAST <i>knock out</i> ( <i>Slc1a3</i> <sup>-/-</sup> ) mouse model.....	16
4.3.3 CIC-2 <i>knock out</i> ( <i>Clcn2</i> <sup>-/-</sup> ) mouse model .....	16
4.3.4 Genotyping.....	16
4.3.5 Animals used for measurements .....	17
4.3.6 Preparation of acute cerebellar slices .....	17
4.4 Fluorescence lifetime imaging microscopy .....	18
4.4.1 Two-photon fluorescence microscope set-up.....	18
4.4.2 Time-correlated single photon counting .....	18
4.5 Characterization of the chloride sensitive fluorescent dye MQAE .....	19
4.5.1 MQAE concentration determination .....	19
4.5.2 Emission spectrum determination.....	19
4.5.3 MQAE fluorescence lifetime measurements in aqueous solution .....	20
4.6 Determination of chloride concentrations.....	22
4.6.1 Calibration of MQAE in pc-astrocytes and Bergmann glia of acute cerebellar slices....	22
4.6.2 Calculation of chloride concentration from MQAE fluorescence lifetimes.....	22
4.6.3 Criteria for analyzed cells.....	23
4.7 Blocker experiments .....	24
4.8 Electrical stimulation .....	24
4.9 Determination of protein expression levels.....	25

4.9.1 Protein extraction .....	25
4.9.2 Determination of protein concentration .....	25
4.9.3 SDS-PAGE .....	26
4.9.4 Western blot .....	26
4.9.5 Immunodetection of proteins.....	26
4.9.6 Chemiluminescence imaging .....	27
4.9.7 Blot analysis .....	27
4.10 Statistical analysis .....	27
4.11 Buffer .....	28
4.11.1 MQAE characterization .....	28
4.11.2 Primary cultured astrocytes (pc-astrocytes).....	28
4.11.3 Acute cerebellar slices .....	29
4.11.4 Protein quantification .....	30
5 Results .....	33
5.1 Determination of $[Cl^-]_{int}$ in primary astrocytic cell culture .....	33
5.2 Determination of the $[Cl^-]_{int}$ in Bergmann glia of acute cerebellar slices.....	36
5.2.1 FLIM imaging in Bergmann glia of acute cerebellar slices .....	36
5.2.2 The role of cation chloride cotransporters in chloride homeostasis of Bergmann glia	38
5.2.3 The effect of chloride channel on the $[Cl^-]_{int}$ of Bergmann glia cells .....	42
5.2.4 The $[Cl^-]_{int}$ in Bergmann glia changes during cerebellar development .....	46
5.2.5 Effects of glutamate and aspartate application on the $[Cl^-]_{int}$ .....	49
5.2.6 Synaptically released glutamate leads to decreased the $[Cl^-]_{int}$ .....	50
5.3 Data.....	53
6 Discussion .....	59

6.1 Intracellular chloride concentrations in cultured astrocytes .....	59
6.2 Intracellular chloride concentrations in Bergmann glia of acute cerebellar slices .....	60
6.3 EAAT1/GLAST and EAAT2/GLT1 regulate intracellular chloride in Bergmann glia and allow dynamic adjustments during glutamatergic synaptic transmission.....	61
6.3.1 Glial EAAT anion channel function affects $[Cl^-]_{int}$ .....	61
6.3.2 EAAT2/GLT1 appears not to be upregulated in <i>Slc1a3</i> <sup>-/-</sup> mice.....	61
6.3.3 EAAT1/GLAST and EAAT2/GLT1 determine the $[Cl^-]_{int}$ during cerebellar maturation...	62
6.3.4 The glial chloride switch in cerebellar Bergmann glia .....	63
6.3.5 Dynamic adjustment of $[Cl^-]_{int}$ performed via glial EAATs during excitatory synaptic transmission .....	63
7 Conclusion .....	65
8 References.....	66
9 Manufacturers.....	75
10 Abbreviations .....	77
11 Eidesstattliche Versicherung .....	81

## List of figures

Figure 3.1	Excitatory amino acid transporters located at a glutamatergic synapse.....	4
Figure 3.2	Schematic illustration of the cerebellar cortex.....	9
Figure 3.3	Jablonski diagram illustrating two photon excitation and collisional quenching.....	12
Figure 3.4	Illustration of the TCSPC underlying mechanism.....	13

Figure 3.5	Chemical structure of the chloride sensitive fluorescent dye MQAE.....	14
Figure 4.1	Absorption and emission spectra of MQAE in intracellular solution (IS).....	20
Figure 4.2	Fluorescence lifetime of MQAE in dependence of different chloride concentrations.....	21
Figure 5.1	Fluorescent intensity and fluorescent lifetime image of MQAE loaded pc-astrocytes.....	34
Figure 5.2	Calibration and determination of the $[Cl^-]_{int}$ of pc-astrocytes.....	35
Figure 5.3	Fluorescence intensity and fluorescence lifetime image of a MQAE loaded acute cerebellar slice.....	37
Figure 5.4	Calibration of the fluorescence lifetime of MQAE and determination of the $[Cl^-]_{int}$ in Bergmann glia of acute cerebellar slices.....	38
Figure 5.5	Fluorescence lifetime image of an acute cerebellar slice incubated with Bumetanide or DIOA, respectively.....	39
Figure 5.6	The $[Cl^-]_{int}$ in acute cerebellar slices incubated with Bumetanide or DIOA, respectively.....	40
Figure 5.7	The effect of cation-chloride-cotransporter blocker Bumetanide and DIOA on the $[Cl^-]_{int}$ in acute cerebellar slices.....	41
Figure 5.8	The $[Cl^-]_{int}$ in Bergmann glia of acute cerebellar slices of <i>Clcn2</i> <sup>-/-</sup> and <i>Slc1a3</i> <sup>-/-</sup> mice.....	43
Figure 5.9	Blocking EAAT1/GLAST and EAAT2/GLT1 directly affects the $[Cl^-]_{int}$ of Bergmann glia in acute cerebellar slices.....	45
Figure 5.10	Quantification of EAAT1/GLAST and EAAT2/GLT1 expression in the cerebellum of WT and <i>Slc1a3</i> <sup>-/-</sup> mice.....	46
Figure 5.11	FLIM images of acute cerebellar slices of young animals of different ages.....	47

Figure 5.12	Calibration and determination of the $[Cl^-]_{int}$ in young animals of wild type and EAAT1/GLAST.....	48
Figure 5.13	Application of high glutamate and aspartate increase the $[Cl^-]_{int}$ of Bergmann glia	49
Figure 5.14	Time dependence of the $[Cl^-]_{int}$ upon electrical stimulation of parallel fibres...	51
Figure 5.15	Effect of electrical stimulation on the $[Cl^-]_{int}$ of Bergmann glia.....	52

## List of tables

Table 4.1	Primers used for genotyping.....	17
Table 4.2	Size of amplified PCR products of the different genotypes.....	17
Table 4.3	Incubation time and concentration of compounds used during the blocker experiments.....	24
Table 4.4	Antibodies used for immunodetection of EAAT1/GLAST, EAAT2/GLT1 and actin.....	26
Table 4.5	Size and isoelectric point of proteins of interest.....	27
Table 5.1	Differences between the $[Cl^-]_{int}$ determined in different experiments and their levels of significance	53
Table 5.2	Stern-Volmer constants ( $K_{SV}$ ) and determination coefficient ( $R^2$ ).....	54
Table 5.3	Values determined for cell populations after blocker application.....	55
Table 5.4	Values determined for different cells of animals of different ages.....	56
Table 5.5	Values determined for cells upon substrate application or electrical stimulation, respectively.....	57
Table 5.6	Relative protein expression levels.....	58

## 1 Abstract

Excitatory amino acid transporters called EAATs are dual function proteins, they are secondary active glutamate transporters as well as anion channels. While the altered anion channel function of glial EAATs is associated with severe human diseases, nothing is known about their physiological role in proper brain function. Glial cells are known to actively accumulate chloride. These cells exhibit a stable negative resting potential, so that anion channels may lower  $[Cl^-]_{int}$  via passive chloride effluxes. Here the role of the glial EAAT isoforms, EAAT1/GLAST and EAAT2/GLT1, for regulating intracellular chloride concentrations in Bergmann glia in the cerebellar cortex was studied using fluorescent lifetime imaging microscopy (FLIM) with the chloride-sensitive fluorescent dye MQAE in acute cerebellar slices. In WT mice and EAAT1/GLAST *knock-out* (*Slc1a3*<sup>-/-</sup>), intracellular chloride concentrations differ significantly (WT = 34.2 mM, *Slc1a3*<sup>-/-</sup> 40.9 mM). A comparable increase in  $[Cl^-]_{int}$  was measured in WT glial cells after isoform-specific blocking of EAAT1/GLAST using UCPH-101. Since, glial EAATs are developmentally upregulated, the age dependence of  $[Cl^-]_{int}$  in Bergmann glia of wild type and *Slc1a3*<sup>-/-</sup> was investigated, and the glial chloride switch was newly-discovered. Starting with high  $[Cl^-]_{int}$  of around 50 mM in young animals, the  $[Cl^-]_{int}$  decreased to the adult level, corresponding to the upregulation of cerebellar EAAT1/GLAST and EAAT2/GLT1 expression. Upon substrate application as well as electrical stimulation dynamic changes in the  $[Cl^-]_{int}$  in Bergmann glia due to glial EAATs could be observed. Changes in the glial  $[Cl^-]_{int}$  may affect secondary active transport over the glial plasma membrane, such as in case of GABA uptake mediated by GAT. Hence, changes in  $[Cl^-]_{int}$  can stimulate the GABA uptake and affect synaptic transmission. Bergmann glia and cerebellar neurons are tightly functional coupled, thus glial EAATs may modulate cell migration during cerebellar maturation and influence synaptic transmission. This work characterized for the first time the cellular function of anion channels associated with EAAT1 and EAAT2. Furthermore, the developmental glial chloride switch in cerebellar Bergmann glia was discovered and characterized.

## 2 Zusammenfassung

Excitatory Amino Acid Transporter (EAATs) sind sowohl sekundär-aktive Glutamat-Transporter, als auch Anionen Kanäle. Während eine Veränderung der Anionen-Kanal-Funktion bereits mit schwerwiegenden humanen Krankheiten in Verbindung gebracht werden konnte, ist ihre physiologische Rolle im gesunden Gehirn noch nicht aufgeklärt. Es ist bekannt, dass Glia aktiv Chlorid akkumulieren und gleichzeitig ein stabiles, negatives Ruhemembranpotential ausbilden, so dass das Öffnen von Anionen Kanälen zu einem passiven Chlorid-Ausstrom führen würde. Im Folgenden wurde die Rolle der glialen EAATs, EAAT1/GLAST und EAAT2/GLT1 auf die intrazelluläre Chloridkonzentration von zerebellären Bergmann Glia mit Hilfe von Fluoreszenz-Lebenszeit-Messungen und dem Chlorid sensitiven Fluorophore MQAE in lebenden cerebellären Schnitten analysiert. Die  $[Cl^-]_{int}$  in WT und EAAT1/GLAST *knock-out* (*Slc1a3*<sup>-/-</sup>) unterscheiden sich signifikant (WT= 34.2 mM, *Slc1a3*<sup>-/-</sup> 40.9 mM). Desweiteren stiegen nach Applikation des EAAT1/GLAST spezifischen Blocker UCPH-101 die  $[Cl^-]_{int}$  auf signifikant höhere Werte an. Da bereits gezeigt werden konnte, dass EAAT1/GLAST und EAAT2/GLT1 altersabhängig hochreguliert werden, wurden die  $[Cl^-]_{int}$  in lebenden, zerebellären Schnitten von Tieren unterschiedlichen Alters bestimmt und dabei der gliale Chlorid-Switch in Bergmann glia neu entdeckt. Beginnend mit einer hohen Chloridkonzentration von etwa 50 mM, sinkt diese mit zunehmendem Alter in Korrelation mit einer Zunahme der Expression von EAAT1/GLAST und EAAT2/GLT1. Sowohl nach Substrat Applikation, als auch nach elektrischer Stimulation wurden dynamische Veränderungen der  $[Cl^-]_{int}$  gemessen. Gliale Zellen nehmen GABA über den GABA-Transporter (GAT) auf, der entlang des Natrium- und des Chlorid-Gradienten transportiert. Veränderte  $[Cl^-]_{int}$  könnten die GABA Aufnahme und somit die synaptische Transmission beeinflussen. Bergmann glia und Neurone sind funktional eng miteinander verbunden, zum einen während der Zellmigration in Jungtieren und zum anderen funktional während der synaptischen Transmission, gliale EAATs können somit beide Funktionen beeinflussen. In dieser Arbeit wird der glialen EAAT-Anionen-Leitfähigkeit zum ersten Mal eine physiologische Rolle zugeordnet und der gliale Chlorid-Switch in zerebellären Bergmann glia zum ersten Mal beschrieben und charakterisiert.

## **3 Introduction**

### **3.1 Excitatory amino acid transporters (EAATs)**

Excitatory amino acid transporters belong to the solute carrier family SLC1 and function as transporter and anion channels. So far, five different mammalian EAAT isoforms have been identified, EAAT1 (GLAST), EAAT2 (GLT1), EAAT3 (EAAC1), EAAT4 and EAAT5 (SLC1A3, SLC1A2, SLC1A1, SCL1A6 and SLC1A7, respectively). They are to 90% identical to the equivalent protein of the other mammalian species (Danbolt, 2001). EAAT1/GLAST and EAAT2/GLT1 are the glial isoforms. Whereas EAAT1 is exclusively expressed in glial cells (Lehre and Danbolt, 1998), EAAT2/GLT1 can be found in some neurons as well (Lehre and Danbolt, 1998, Schmitt et al., 1996). The neuronal isoforms EAAT3 and EAAT4 are located in dendrites and spines. EAAT4 is the major glutamate transporter in neurons (Dehnes et al., 1998) and EAAT5 is mainly found in the retina, where it is expressed in photoreceptors and bipolar cells (Lee et al., 2013).

EAATs are high-affinity, secondary-active glutamate transporters, which mediate stoichiometrically coupled cotransport of one glutamate, one proton and three sodium ions against one potassium ion (Levy et al., 1998, Zerangue and Kavanaugh, 1996). Furthermore, EAATs also function as anion-selective channels (Fairman et al., 1995). The anion selective conduction pathway is formed during an intermediate state of the glutamate transport cycle (Machtens et al., 2015). The major role of these dual function proteins is to clear the excitatory neurotransmitter glutamate from the synaptic cleft and terminate glutamatergic synaptic transmission. They help sustain a high signal to noise ratio and simultaneously EAATs keep the extracellular glutamate concentration below a neurotoxic level (Danbolt, 2001).

The five mammalian EAATs differ in their glutamate transport rates and their anion currents. EAAT1/GLAST and EAAT2/GLT1 are described as efficient transporters with small macroscopic anion currents (Mim et al., 2005), consequently, it was shown that the glial EAAT isoforms are responsible for the major part of glutamate uptake (Bergles et al., 1997, Danbolt, 2001). EAAT3, 4 and 5 predominantly conduct anions and are low capacity transporters (Mim et al., 2005).

The glutamate transport function of all isoforms has already been extensively studied (Danbolt, 2001), while the physiological role of the EAAT anion channel function is still not fully

understood. For neuronal EAATs a role as negative feedback on presynaptic excitability at glutamatergic synapses was proposed (Wersinger et al., 2006, Veruki et al., 2006), whereas in glia their role remains unknown. Many physiological tasks of glia are linked to transmembrane ion gradients, therefore, intra- or extracellular ion concentrations are important determinants of these properties, and can be influenced by EAAT anion channel function.

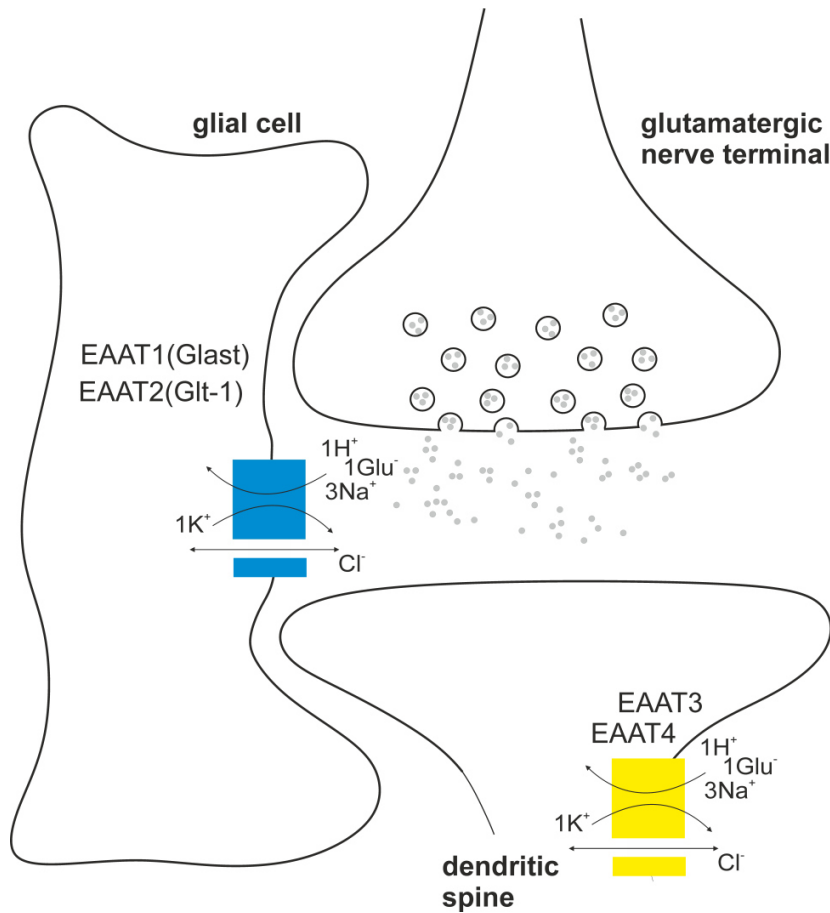


Figure 3.1: **Excitatory amino acid transporters located at a glutamatergic synapse.** A: The isoforms EAAT1/GLAST and EAAT2/GLT1 are located in the glial plasma membrane and transport glutamate upon synaptic release. The isoforms EAAT3 and EAAT4 are located in the neuronal membrane at the dendritic spine. Modified from Danbolt, 2001.

EAAT2/GLT1 is most abundant in all regions of the mammalian central nervous system (CNS) except for regions where EAAT1/GLAST is mainly expressed (Lehre and Danbolt, 1998). Both isoforms are described to be evenly distributed over the astrocytic plasma membrane, with the

exception of glial to glial membranes, where less transporters are located (Chaudhry et al., 1995).

### **3.2 The role of glial EAAT isoforms in diseases**

The isoforms EAAT1/GLAST and EAAT2/GLT1 were discovered to play a role in pathological conditions leading to severe symptoms. Recently, a missense mutation in EAAT1/GLAST was associated to the human disease episodic ataxia 6 (EA6). While the malfunction of the mutated protein has been described (Winter et al., 2012) the pathomechanism remains unknown. In the case of EAAT2/GLT1 the genetic ablation of the protein leads to lethal spontaneous seizures and increased susceptibility to acute cortical injury (Tanaka et al., 1997).

#### **3.2.1 Altered EAAT1/GLAST anion conduction is associated with episodic ataxia and epilepsy**

A patient showing episodes of ataxia, epileptic seizures, headache, and brain oedema is heterozygous for the substitution of the highly conserved proline at position 290 by an arginine in EAAT1/GLAST (Jen et al., 2005). Episodic ataxia (EA) is a human genetic disease characterized by paroxysmal cerebellar incoordination. EA6 is one of seven different forms of episodic ataxia that have been described so far (Jen et al., 2007). The effect of the mutation P290R in EAAT1/GLAST was studied in heterologous expression systems, gain of function in anion conductance and reduction of glutamate transport-rates were identified (Winter et al., 2012). In presence, as well as in absence of glutamate, anion currents are significantly increased (Winter et al., 2012). Surprisingly the EAAT1/GLAST *knock-out* (*Slc1a3*<sup>-/-</sup>) mouse shows neither epileptic seizures nor episodes of ataxia. Extracellular glutamate concentrations are within the physiological range and motor coordination is just slightly impaired (Watase et al., 1998). Thus, the severe symptoms described in the EA6 patient are not linked to reduced glutamate transport rates. It appears to be the increased anion conductance which leads to episodes of ataxia and is involved in triggering epileptic seizures.

#### **3.2.2 The loss of glial EAAT2/GLT1 leads to lethal spontaneous seizures in mice**

Deletion of EAAT2/GLT1 eliminates around 95% of the glutamate uptake activity and leads to premature death due to intractable seizures (Tanaka et al., 1997). Recently, two conditional

EAAT2/GLT1 *knock-out* mice were generated in which EAAT2/GLT1 expression is inactivated in astrocytes or in neurons, respectively (Petr et al., 2015). This study revealed for the glial specific *knock-out* only slightly, insignificant increases in extracellular glutamate levels, albeit the animals suffered from seizures, lower body weight and increased mortality. In contrast the neuron specific knockout mouse showed no seizures, normal survival and weight gain, but the glutamate uptake capacity was significantly decreased by around 40% (Petr et al., 2015). Thus, the severe phenotype in the glial EAAT2/GLT1 *knock-out* appears not to be due to the missing glutamate transport. Rather it could be the missing EAAT2/GLT1 anion channel function which contributes to the origin of the described symptoms.

### **3.3 Working hypothesis**

The involvement of glial EAAT anion channel function in severe diseases gives the hint that EAAT anion channels play an important role in brain function. They may affect the intracellular chloride concentration and thereby change electrochemical gradients. This work investigates the cellular role of glial EAAT anion channel function and their effects on intracellular chloride concentrations. In animals of different ages and under different physiological conditions the effect of glial EAAT anion channel function was characterized. Furthermore, the role of other chloride channels and transporters on intracellular chloride of glial cells was analyzed to classify the contribution of glial EAATs on chloride homeostasis.

### **3.4 The cerebellum is the predominant expression site of EAAT1/GLAST**

EAAT1/GLAST is predominantly expressed in the cerebellum, whereas EAAT2/GLT1 expression is much lower (Lehre and Danbolt, 1998). The cerebellum is involved in movement, long term learning and cognitive functions such as language. It plays a central role in motor control and contributes to coordination, precision and accurate timing of movement. Cerebellar dysfunction leads to disorders in fine movement, posture, equilibrium, and motor learning. Furthermore, it causes symptoms such as ataxia, tremor, nystagmus or imbalance (Sultan, 2014, Glickstein et al., 2011).

#### **3.4.1 Cerebellar morphology**

The cerebellum is composed of white matter, containing the deep cerebellar nucleus, and the cerebellar cortex. The cerebellar cortex consists of three different cell layers, the molecular, Purkinje cell, and the granule cell layer. The granule cell layer harbours the granule cells and a second type of neurons, the Golgi cells. The Purkinje cells are the output neurons of the cerebellum and are located in the Purkinje cell layer, on top of the granule cell layer. In between, the Bergmann glial cells are located, the major expression site of EAAT1/GLAST. Purkinje cells and Bergmann glial fibres spread outwards through the molecular layer, which contains neuronal basket cells and stellate cells as well as parallel fibres, outgrowing from the granule cells (Braitenberg and Atwood, 1958, Glickstein et al., 2009, Sultan, 2014).

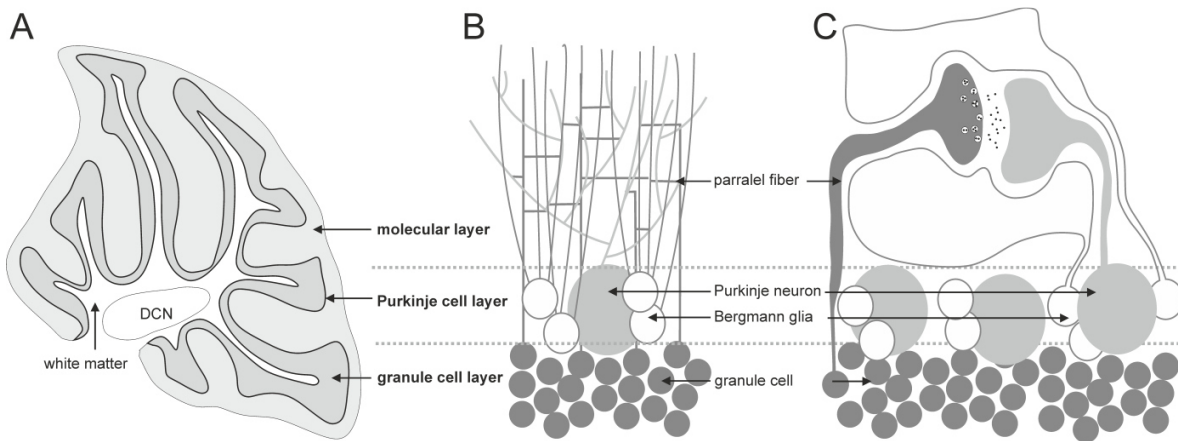


Figure 3.2: **Schematic illustration of the cerebellar cortex.** A: Sagittal plane of the mouse cerebellum. The white matter harbours the deep cerebellar nucleus (DCN) and the cortex consists of three layers: granule cell layer, Purkinje cell layer and molecular layer. B: Sagittal plane of the cerebellar cortex with the granule cell layer, containing granule cells; the Purkinje cell layer, containing Purkinje neurons and Bergmann glia; and the molecular layer, harbouring parallel fibres, Bergmann glia and Purkinje cell fibres. C: Illustration of the signal input coming from granule cells through parallel fibres, the following glutamate release at a parallel fibre Purkinje neuron synapse and signal output through the Purkinje neuron. The synapse is sheathed with Bergmann glia. Modified from Tanaka et al., 2008, Tzingounis and Wadiche, 2007.

### 3.4.2 Cerebellar signalling circuit

The cerebellum receives input from the outside via mossy fibres and climbing fibres. Both signal directly to the deep cerebellar nucleus (DCN), the output region of the cerebellum, as well as to the neurons of the cerebellar cortex (Shinoda et al., 2000). Purkinje cells receive input from one climbing fibre, and several inputs from granule cells via their parallel fibres, which obtain input from mossy fibres and spread through the molecular layer to build synapses with the Purkinje cells (Shinoda et al., 2000). These synapses between Purkinje cells and climbing fibres as well as parallel fibres are sheathed by Bergmann glial microdomains (Grosche et al., 1999). The output signal is generated by the Purkinje cells which spread their axon down to the white matter onto deep cerebellar neurons (Ito et al., 1970).

### 3.5 Chloride homeostasis of Bergmann glia

The intracellular chloride concentration of Bergmann glia seems to be a crucial property for accurate function in the cerebellar network. Cerebellar Bergmann glia exhibits a stable

negative resting potential which is generated by a predominant resting potassium conductance and assumes values close to the potassium reversal potential (Bergles et al., 1997). It was shown that glial cells have higher intracellular chloride concentrations (Bekar and Walz, 2002), as expected in case of passive diffusion. Thus Bergmann glia are supposed to actively accumulate chloride. Changes in intracellular chloride concentrations will modify regulatory volume decreases and increases, a crucial condition during cell migration in the immature brain (Schwab et al., 2012, Habela et al., 2009). Furthermore, changed intracellular chloride concentrations modify the driving force for secondary-active transporters utilizing transmembrane chloride gradients. For example, GABA uptake by Bergmann glia via GAT (Zhou and Danbolt, 2013), is driven by sodium and chloride gradients. This can change the extracellular GABA concentration, which may affect synaptic transmission and has been reported to influence cell migration (Luhmann et al., 2015).

### **3.5.1 Chloride accumulation in Bergmann glia**

Electroneutral cation-chloride cotransporters belonging to the solute carrier family SLC12 are involved in adjusting intracellular chloride in different cell types (Gagnon, Payne). The  $\text{Na}^+\text{-K}^+\text{-Cl}^-$  cotransporters (NKCCs) depend on the transmembrane gradient of  $\text{Na}^+$  and  $\text{K}^+$ , and are inwardly directed. K-Cl cotransporters (KCCs) are  $\text{K}^+$  dependent  $\text{Cl}^-$  transporters and outwardly directed. In the central nervous system, the gene family of cation chloride cotransporters (CCCs) is represented by KCC1-3 and NKCC1. The balance between  $\text{Cl}^-$  extruding KCCs and  $\text{Cl}^-$  accumulating NKCCs may take part in regulating intracellular chloride concentration of glial cells. Bergmann glia express transporters of both types, NKCC1, KCC1, and KCC3 (Yan et al., 2001, Mount et al., 1999, Mikawa et al., 2002, Kanaka et al., 2001, Hubner et al., 2001).

### **3.5.2 Anion channels in Bergmann glia**

Next to EAAT1/GLAST and EAAT2/GLT1 Bergmann glia express further types of chloride channels. These consist of voltage-gated  $\text{Cl}^-$  channels, which are a member of the CLC family (Hoegg-Beiler et al., 2014); and the volume activated anion channels, VRAC and VSOC (Hydzinski-Garcia et al., 2014). Since Bergmann glia exhibit a stable negative resting potential, in

presence of active chloride accumulation, the opening of chloride channels can lower  $[Cl^-]_{int}$  via passive chloride effluxes. The EAATs anion conductance is increased in presence of glutamate; thus, chloride efflux could be increased during glutamatergic synaptic transmission. For glial EAAT isoforms 1 and 2, an age-dependent increase in expression levels has been described in hippocampal and somatosensory astrocytes as well as in the rat cerebellum (Regan et al., 2007, Schreiner et al., 2014, Voutsinos-Porche et al., 2003, Ullensvang et al., 1997, Holmseth et al., 2012). ClC-2 was found to be expressed in astrocytes (Sik et al., 2000, Nobile et al., 2000). It is activated below the resting membrane potential, during cell swelling and extracellular acidification (Jordt and Jentsch, 1997). This channel appears to be suited for chloride regulation (Staley et al., 1996). The ClC-2 *knock-out* (*Clcn2*<sup>-/-</sup>) mouse shows a retinal degeneration and homozygous males are infertile (Bosl et al., 2001). In addition, a brain vacuolation phenotype was observed in older animals (Blanz et al., 2007), however, no ataxic or epileptic phenotype has been described.

### **3.6 Chloride imaging**

#### **3.6.1 Fluorescence lifetime imaging microscopy**

Fluorescence lifetime imaging microscopy with two-photon excitation is a suitable tool to determine chloride concentrations of living cells in tissue slices. It is non-invasive, independent of the dyes fluorescent intensity and works at a high spatial resolution. Thus, this optical method is uniquely suited for measuring intracellular chloride concentrations (Kaneko et al., 2004, Gilbert et al., 2007, Gensch et al., 2015).

Fluorescence is a form of luminescence and results from the emission of light by an excited fluorophore. In the excitation process, photon absorption transfers the fluorophore from the ground ( $S_0$ ) to an excited state (e.g.  $S_1$ ). The average time a fluorophore stays in  $S_1$ , before returning to  $S_0$ , defines the fluorescence lifetime ( $\tau$ ). The emission rate of fluorophores is usually between  $10^{-8}$  to  $10^{-9} \text{ s}^{-1}$ , resulting in general in a fluorescence lifetime of around 1-10 ns. The fluorescence lifetime can be measured by time-correlated single photon counting (TCSPC) (Becker, 2005).

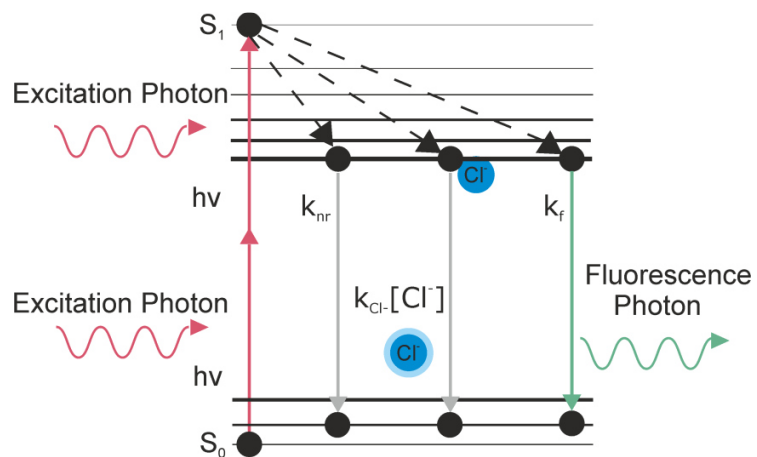


Figure 3.3: **Jablonski diagram illustrating two photon excitation and collisional quenching.** A fluorophore can be excited either by one photon or by two or more photons, which impinge on the fluorophore at the same time and provide the same energy, as the photon in the case of one photon excitation. The fluorophore stays in the excited state ( $S_1$ ) for the characteristic fluorescence lifetime ( $\tau$ ) until it returns to the ground state ( $S_0$ ) either by emission of light ( $k_f$ ) or by non-radiative decay ( $k_{nr}$ ). In case of collisional quenching the fluorophore can collide with the quencher (here chloride) and return to the ground state without emission of light ( $k_q$ ).

### 3.6.2 Measuring fluorescence lifetimes using time correlated single photon counting

In the technique of TCSPC the probe is excited with a sequence of photon pulses (length: 50 fs – 200 ps). The photon pulses are typically generated by pulsed lasers with defined wavelength, pulse length and pulse repetition frequency. The latency between excitation and detection of single photons is measured. These so-called arrival times are registered in a histogram to determine the average fluorescence lifetime. The plotted fluorescence lifetimes usually result in an exponential distribution.

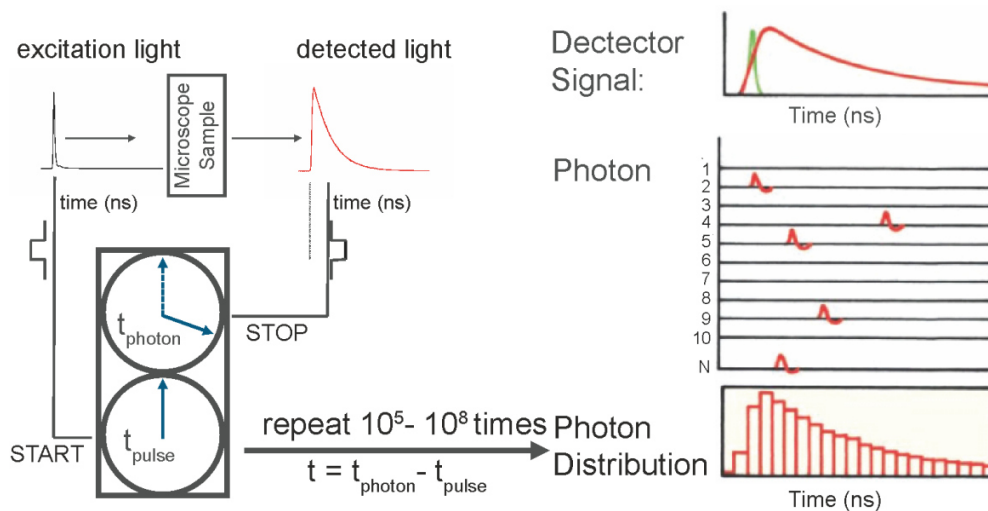


Figure 3.4: **Illustration of the TCSPC underlying mechanism.** The average fluorescence lifetime is measured by counting single photons and measuring the time it takes them to excite the fluorophore and to be detected after emission. In total  $10^5$  to  $10^8$  photons are collected and stored in a histogram to calculate the average fluorescence lifetime. Modified from Becker, 2005.

### 3.6.3 The chloride sensitive fluorescent dye MQAE

MQAE (1-(Ethoxycarbonylmethyl)-6-methoxyquinolinium bromide) is a quinolinium-derivate with chloride concentration sensitive fluorescence properties. This dye is collisional quenched by chloride, if the excited fluorophore collides with chloride it returns to the ground state without emission of light (see the chloride dependent deactivation pathway of S1 in figure 3.3). Due to this property, the fluorescence lifetime of MQAE is inversely proportional to the chloride concentration. The same is true for the fluorescence intensity of MQAE, however the fluorescence lifetime is still the preferred readout parameter, since the fluorescence intensity depends on the amount of MQAE in the cell and the excitation light intensity.  $K_{SV}$  and  $\tau_0$

(fluorescence lifetime at zero quencher concentration) are parameters specific for MQAE depending on the surrounding environment because MQAE is not only quenched by chloride but by other anions as well. Due to the very high  $K_{SV}$ , different chloride concentrations result in detectable changes in the average fluorescence lifetime, which makes MQAE a well-suited fluorescent dye for FLIM studies.

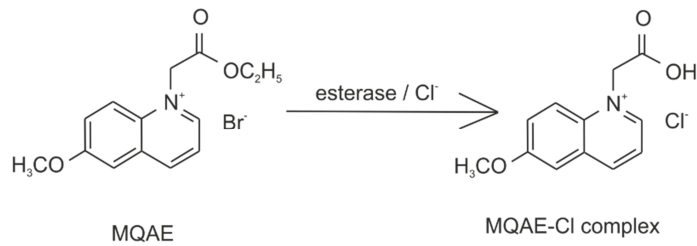


Figure 3.5: **Chemical structure of the chloride sensitive fluorescent dye MQAE.** MQAE is an AM-ester that can penetrate the cellular membrane by diffusion. Intracellular esterases hydrolyze MQAE, which then becomes membrane impermeable and intracellular trapped. MQAE is collisionally quenched by chloride.

### 3.6.4 Two photon microscopy

In the case of one photon excitation a fluorophore is excited by one photon of light of a certain energy and a specific wavelength ( $E = \frac{h \cdot c}{\lambda}$ ). The energy, which is needed to excite the fluorophore, can be provided by more than one photon as well. As long as the total energy absorbed by the fluorophore yields the same energy and the photons impinge on the fluorophore within a very short time period ( $10^{-16}$  s). This leads to spatial limitation of excitation, which occurs only in the focus area and, thus, leads to less background fluorescence and reduced photo-toxicity. No excitation occurs in out-of-focal plane layers in contrast to conventional one-photon excitation as in popular confocal scanning microscopy. For two-photon excitation, in general, photons at a wavelength of approximately half the energy are used. Light of a longer wavelength is less scattered and causes less photo damage toxicity. Scattering is the main limitation for tissue imaging. The less scatter occurs, the deeper the light enters the tissue, and imaging of deeper cell layer can be achieved.



## **4 Materials & Methods**

### **4.1 Chemicals and materials**

All chemicals and solutions were at least purity p.a. and obtained from different companies, which are listed in chapter 9. For all solutions and buffers bi distilled water was used.

### **4.2 Cell culture**

#### **4.2.1 Primary cultured astrocytes (pc-astrocytes)**

For in vitro analysis of the role of EAAT1/GLAST anion channel function, primary culture of EAAT1/GLAST expressing astrocytes was produced from whole brain preparation.

##### **4.2.1.1 Isolation and cell maintenance**

Mice of the wild type strain C57bl6 were anesthetized with isoflurane and decapitated. The whole brain was removed quickly and astrocytes were isolated by magnetic-beads and an anti-GLAST antibody as described elsewhere (Jungblut et al., 2012) using the Anti-GLAST MicroBead Kit (130-095-825, MACS Milteny Biotec). These cells – from now on named pc-astrocytes – were cultured in serum-free media supplemented with heparin-binding epidermal growth factor (HBEGF) on glass cover slips (Foo et al., 2011). Every second day the medium was renewed.

##### **4.2.1.2 Imaging**

Between 5 and 26 days in vitro (DIV), cells were washed with phosphate buffered saline (PBS) and incubated with 5 mM MQAE, dissolved in extracellular solution (ES), for 30 min at 37° C in the incubator. Afterwards, the cells were rinsed with PBS again and imaged in 3 cm plastic dishes containing ES.

## **4.3 Animals**

### **4.3.1 Mice maintenance**

Mice were housed under standard conditions in the animal facility of the Forschungszentrum Jülich (FZJ) according to institutional guidelines and kept on a 12 h light/dark cycle. All experiments were approved and in compliance with the German Law for Protection of Animals, the FZJ and the Landesamt für Natur, Umwelt und Verbraucherschutz (LANUV) of North-Rhine Westphalia (Reference number 84-02.04.2014.A334).

### **4.3.2 EAAT1/GLAST knock out (*Slc1a3*<sup>-/-</sup>) mouse model**

Heterozygous EAAT1/GLAST<sup>+/-</sup> (*Slc1a3*<sup>+/-</sup>) were obtained from Dr. Niels Danbolt (Institute of Basic Medical Science, University of Oslo) and generated as described before (Watase et al., 1998) in a C57black6 (B6.129P2) background. Heterozygous animals were bred since homozygous knock-out animals show poor nesting behaviour. For genotyping, the primers GLAST-KO-A, GLAST-KO-B, GLAST-KO-C and GLAST-KO-D were used (table 4.1).

### **4.3.3 CIC-2 knock out (*Cicn2*<sup>-/-</sup>) mouse model**

Pregnant homozygous CIC-2<sup>-/-</sup> (*Cicn2*<sup>-/-</sup>) females were obtained from Dr. Holger Lerche (Zentrum für Neurologie, Hertie Institut für klinische Hirnforschung, Tübingen, Germany). The females were mated with heterozygous males, since homozygous males are infertile. For genotyping the primer combinations CIC2KO-F, CIC2-NeoKO-F and CIC2KO-R were used (table 4.1).

### **4.3.4 Genotyping**

Genotypes were determined by polymerase chain reaction (PCR) from DNA obtained from tail biopsies using the KAPA Mouse Genotyping hot start kit (Peqlab) and primers as referenced in table 4.1. Amplified PCR products were analyzed on a 1.5% agarose gel, 25 min, 80 V, 200 mA and their size (compare to table 4.2) compared to a 100 bp gene ruler (Thermo Scientific, SM0241).

Table 4.1: **Primers used for genotyping** (All primers were manufactured by Eurofins Genomics).

Primer	Sequence
GLAST-KO-A	AAGTGCCTATCCAGTCCAACGA
GLAST-KO-B	AAGAACTCTCTCAGCGCTTGCC
GLAST-KO-C	AATGGAAGGATTGGAGCTACGG
GLAST-KO-D	TTCCAGTTGAAGGCTCCTGTGG
CIC2KO-F	ATGTATGGCCGGTACACTCAGGAACTC
CIC2-NeoKO-F	CCTGGAAGGTGCCACTCCCCTGTCC
CIC2KO-R	ACACCCAGGTCCCTGCCCAATCTGG

Table 4.2: **Size of amplified PCR products of the different genotypes using the corresponding primers** (table 1).

Genotype	PCR fragment
<i>Slc1a3</i> <sup>-/-</sup>	383 bp
EAAT1/GLAST WT	214 bp
<i>Cln2</i> <sup>-/-</sup>	~300 bp
CIC-2 WT	~200 bp

#### 4.3.5 Animals used for measurements

Slice preparation was performed with animals of either sex. Exclusively homozygous *Slc1a3*<sup>-/-</sup>, *Cln2*<sup>-/-</sup> and wild type animals were used for measurements. All experiments were performed with animals at the age of P20-P30, if not noted differently. Details are indicated in the respective experimental chapters.

#### 4.3.6 Preparation of acute cerebellar slices

Acute cerebellar slices were prepared as described earlier (Edwards et al., 1989). After anesthetizing the mouse with isoflurane, and decapitation, the brain was rapidly removed from the skull and placed in ice-cold Preparation-Ringer's solution. Sagittal cerebellar slices of 250 µm thicknesses were cut at 4° C with a Microm (HM650V, Thermo Scientific, frequency 60, amplitude 1, drive 10 P18-P100, drive 8-9 P5-P13) and transferred to a gaze slice holder basket

arranged in oxygenated Preparation-Ringer's solution at 37°C. After 30 min, slices were transferred to oxygenated Normal-Ringer's solution at room temperature (20 – 22° C) and stored for at least 90 min (Meier et al., 2006) until usage. During all experiments, solutions were constantly oxygenated with carbogen (5% CO<sub>2</sub> in O<sub>2</sub>). After 90 min of regeneration time in Normal-Ringer's solution, slices were transferred in Normal-Ringer's solution containing 5 mM MQAE (1-(Ethoxycarbonylmethyl)-6-methoxyquinolinium bromide, Sigma, (Verkman et al., 1989)) and incubated for 30 min at room temperature. The loaded slices were rinsed with MQAE free Normal-Ringer's solution before imaging.

#### **4.4 Fluorescence lifetime imaging microscopy**

##### **4.4.1 Two-photon fluorescence microscope set-up**

MQAE loaded slices were transferred to an imaging chamber placed on the stage of an upright scanning fluorescence microscope (A1 MP; Nikon Instruments Europe) equipped with a 25 × water-immersion objective (NA 1.1 and working distance 2.0 mm; Nikon). Fluorescence was excited by 100 fs light pulses ( $\lambda_{exc} = 750$  nm (Marandi et al., 2002)) by two-photon excitation. Laser pulses were generated at a frequency of 80 MHz by a mode-locked Titan-Sapphire laser (MaiTai DeepSee; output power 2.3 W at 750 nm; Newport Spectra Physics). The laser light was directed onto the cerebellar slice through the lens with reduced power of around 5 mW. The focal spot is scanned over the sample to generate a 512 x 512 pixel raster-image (pixel size: 0.33  $\mu$ m). Fluorescence was filtered by a filter separating MQAE fluorescence (em: 460 nm) from autofluorescence (short pass filter, 500 nm,  $\lambda_{obs} < 510$  nm; Omega Optical) and recorded by a GaAsP hybrid photodetector (HPM-100-40; Becker & Hickl).

##### **4.4.2 Time-correlated single photon counting**

For fluorescence lifetime imaging, time-correlated single photon counting electronics (SPC152; Becker & Hickl) and acquisition software (SPCM 9.67; Becker & Hickl) were used (Gilbert et al., 2007, Kaneko et al., 2004). Lifetime images were analyzed using SPCImage 4.8 (Becker & Hickl) by fitting a bi-exponential model equation to the fluorescence decay in every pixel (bin five) of the image.

## 4.5 Characterization of the chloride sensitive fluorescent dye MQAE

### 4.5.1 MQAE concentration determination

To measure the absorption spectra of MQAE, a UV-2450 absorption spectrophotometer (Shimadzu) was used. The absorption spectrum is plotted in figure 4.1 in black and shows two maxima at 320 nm and 350 nm. The MQAE concentration was determined using the Lambert-Beer law. A sample of the stock solution was filled into a quartz cuvette (0.2 cm x 1 cm x 4 cm) to measure the absorption profile. The exact concentration was calculated by comparison of the absorption maximum of the diluted dye, with the absorption of pure solution under identical conditions:

$$A = c * \varepsilon * d \quad (1)$$

$$c[M] = \frac{Abs(MQAE - solution) - Abs(solution)}{d[cm] * \varepsilon [cm^{-1}M^{-1}]} \quad (2)$$

with  $d$  being the optical path in the cuvette (1 cm), and  $\varepsilon$  the extinction coefficient ( $2800 M^{-1}cm^{-1}$  at 350 nm (Verkman et al., 1989)).

### 4.5.2 Emission spectrum determination

Fluorescence spectra were recorded using a Quanta-Master 40 fluorescence spectrophotometer (Photon Technology International). The wavelength of MQAEs absorption at 380 nm was applied, the resulting spectra were recorded and plotted using the software FeliX32 (Photon Technology International). The emitted light is described by the grey curve in figure 4.1, which shows one broad maximum at 460 nm.

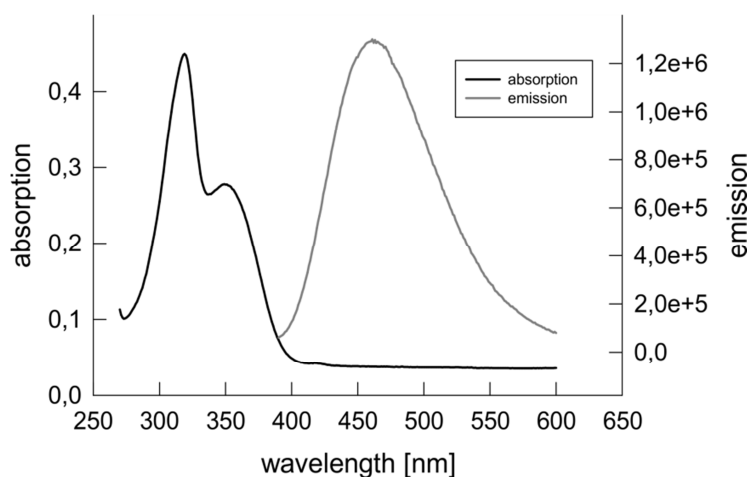


Figure 4.1: **Absorption and emission spectra of MQAE in Intracellular solution (IS)**. The absorption spectrum of MQAE is shown in black with the corresponding y-axis scale bar on the left, while the emission spectrum is plotted in grey with the y-axis scale bar on the right (ex: 380 nm).

#### 4.5.3 MQAE fluorescence lifetime measurements in aqueous solution

MQAE is collisionally quenched by chloride, and this property causes a dependence of the fluorescence lifetime on the surrounding chloride concentration (equation 3).

$$\frac{\tau_0}{\tau} = 1 + K_{SV} [Cl^-] \quad (3)$$

$K_{SV}$  (Stern-Volmer constant) and  $\tau_0$  (fluorescence lifetime at the absence of  $Cl^-$ ) are parameters specific for MQAE depending on the surrounding environment. If possible, both parameters should be determined in the particular environment. The time-resolved detection of the fluorescence intensity decay of MQAE in presence of different chloride concentrations was performed using a Fluotime100 fluorescence spectrophotometer (Picoquant) based on a picoHarp300 TCSPC unit by using a pulsed LED (Laser Picoquant PLS 370, emission 381 nm; pulse width: 450 ps; repetition frequency: 20 MHz) as an excitation source. Fluorescence decay curves as a function of time,  $I(t)$ , were measured by time-correlated single-photon counting (TCSPC). That enables the determination of fluorescence decay components with fluorescence lifetimes greater than 100 ps (Geiger et al., 2012, Becker, 2005). The fluorescence lifetime was determined for the same probes by collecting fluorescence intensity decays with 10000 counts in the maximum (exc: 380 nm; obs: 460 nm). The internal response function (IRF) was

measured by illuminating water at a wavelength of 380 nm and detecting scattered photons at a wavelength of 379 nm.

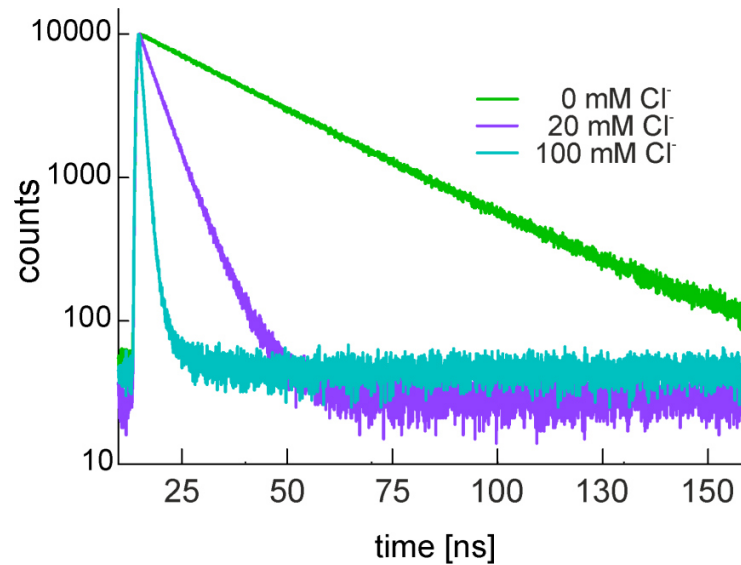


Figure 4.2: **Fluorescence lifetime of MQAE in dependence of different chloride concentrations.** The fluorescence intensity decay of MQAE in the presence of different chloride concentrations (0, 20, and 100 mM), indicated by different colors is plotted.

Decay curves were analyzed by iterative re-convolution of the instrument response function,  $IRF(t)$ , with an exponential model function,  $M(t)$ , using the FluoFit software (version 4.5.3.0; Picoquant) applying equations (4) and (5):

$$I(t) = IRF(t) * M(t) \quad (4)$$

$$M(t) = \sum_{i=1}^n [a_i * \exp\left(-\frac{t}{\tau_i}\right)] \quad (5)$$

$\tau_i$  is the characteristic lifetime and  $a_i$  is the respective intensity;  $n$  (= 1 or 2) is the number of decay functions. Usually one decay function is applied per fluorophore, but in the case of MQAE a bi-exponential decay fits the decays best. Especially in cells, a bi-exponential fit has significantly lower residuals. There are different reasons for the more complex decay behaviour of MQAE, one being the different conformations of the fluorophore, and another being that in cells the hydrolysed as well as the non-hydrolysed form of MQAE can be found, both showing different decay properties.

The average fluorescence lifetime,  $\tau_{fl,ave}$ , was calculated using equation (6).

$$\tau_{fl,ave} = \frac{\sum_{i=1}^n (a_i * \tau_i)}{\sum_{i=1}^n a_i} \quad (6)$$

## 4.6 Determination of chloride concentrations

### 4.6.1 Calibration of MQAE in pc-astrocytes and Bergmann glia of acute cerebellar slices

Due to the fact that MQAE is not only quenched by chloride, the average fluorescence lifetime measured in different cells cannot be directly compared. To calculate chloride concentrations from the measured fluorescence lifetimes, the cell specific Stern-Volmer constants must be determined. For MQAE calibration cells were first washed in HEPES-buffered KCl and K-gluc solution containing different chloride concentrations (0 to 140 mM). Afterwards, the solution was supplemented with 10  $\mu$ M Nigericin (Nigericin sodium salt, Sigma) and 10  $\mu$ M Tributyltin (Tributyltin chloride, Sigma) to equalize inner and outer chloride concentrations (Kovalchuk and Garaschuk, 2012), since Nigericin exchanges  $K^+$  and  $H^+$ , and Tributyltin antiports  $Cl^-$  and  $OH^-$ . If the intra- and extracellular  $K^+$  concentration are the same, the cytosolic chloride concentration equals to that of the corresponding extracellular calibration solution (Krapf et al., 1988, Marandi et al., 2002). Accordingly, the fluorescence lifetime of MQAE was calibrated in pc-astrocytes and in Bergmann glia of acute cerebellar slices.

### 4.6.2 Calculation of chloride concentration from MQAE fluorescence lifetimes

A linear regression, using a least square fit, of the Stern-Volmer analysis of average fluorescent lifetimes for different chloride concentrations (0, 20, 40, 60, 80 and 140 mM) provided the Stern-Volmer constant ( $K_{SV}$ ) of MQAE in Bergmann glia ( $17 M^{-1}$ ). To determine the  $K_{SV}$  for MQAE in pc-astrocytes the fluorescence lifetimes were plotted as  $1/\tau$  ( $t = 4, 20, 40, 60, 80,$  and  $100$  mM). The data were fitted, using a nonlinear least square fit and  $\tau_0$  was calculated.  $K_{SV}$  was then determined as described for Bergmann glia before ( $6.6 M^{-1}$ ). The fluorescence lifetime of all cells was determined by setting a region of interest (ROI) around the soma in SPCImage 4.8 and calculating the mean value of the average fluorescence lifetime of all pixels in the ROI

(usually representing a single cell). This value was then used to calculate the corresponding chloride concentration by equation (7).

$$[Cl^-]_{int} = \frac{\tau_0 - \tau}{K_{SV}} \quad (7)$$

with  $\tau_0$  being the fluorescence lifetime at a chloride concentration of 0 mM chloride,  $\tau$  the average fluorescence lifetime of the ROI, and  $K_{SV}$  the corresponding Stern-Volmer constant. The coefficient of determination is notated by  $R^2$ . This value indicates how well the data fit the regression model and can range from 0 to 1, while 1 means a perfect fit and 0 that the regression is not suitable at all.

#### 4.6.3 Criteria for analyzed cells

During slice preparation the tissue is cut with a blade, thus, cells in close proximity to the cutting edge will be damaged. Per measurement several cells are imaged at the same time, which were loaded via passive diffusion in a solution containing the fluorescent dye. To make sure that during all different experimental conditions just healthy, efficiently loaded cells were considered for analysis, the following criteria were used. Slices were prepared using the whole cerebellum of a mouse. Each measurement took around 15 minutes and 3 to 4 images were taken per slice in the depth of the third to fifth Bergmann glial cell layer from the upper cutting edge. All cells that could be identified as Bergmann glial cells, due to their characteristic morphology (cell size and position between Purkinje cells in the Purkinje cell layer) and were sufficiently loaded with MQAE (determined by the fluorescence intensity level at excitation with constant laser power), were analyzed. Recordings during which the slices moved in x, y or z direction were excluded from the analysis, as well as slices that lay askew, with respect to the imaging plane of the microscope. In the case of electrical stimulation, only cells that could be identified before and after the stimulation were analyzed.

## 4.7 Blocker experiments

To emphasize the specific roles of different transporter types and ion channels in the regulation of  $[Cl^-]_{int}$  in Bergmann glia, different blocker compositions were applied. All blocker experiments were initiated with control recordings ( $n = 2 - 3$ ) under physiological conditions. Slices were incubated in blocker containing Normal-Ringer's solution prior to measurements and constantly perfused with the same solution during the measurement. Blocker reagents were diluted in Normal-ringer's solution, and incubation and perfusion occurred under permanent oxygenation. Blocking experiments were performed with adult animals at the age of P20 - P30. In the case of UCPH-101 slices were incubated with this blocker for 10 minutes before use and perfused with Normal-Ringer's solution without additional blocker during chloride imaging. UCPH-101 exhibits very slow unblocking kinetics (Abrahamsen et al., 2013) and is not washed out within the measurements that lasted around 15 minutes. The detailed concentrations and measurement protocols for all blockers are listed below (table 4.3).

Table 4.3: Incubation time and concentration of compounds used during the blocker experiments.

Blocker	Concentration	Incubation [min]
L-glutamate (Sigma Aldrich)	500 $\mu$ M	60
R-(+)-DIOA (Santa Cruz biotechnology)	80 $\mu$ M	20
DL-TBOA (TOCRIS)	100 $\mu$ M	15
UCPH-101 (Abcam)	10 $\mu$ M	10
Bumetanide (Sigma Aldrich)	40 $\mu$ M	10
D-aspartate (Sigma Aldrich)	1 mM	5-30

## 4.8 Electrical stimulation

For electrical stimulation a bipolar electrode was applied and parallel fibre activity was mimicked by characteristic electrical pulses (van Beugen et al., 2013). Every stimulation experiment was initiated with control recordings ( $n = 2 - 3$ ) under physiological conditions. Electrical stimulation of parallel fibres (PF) was performed by square pulses (150  $\mu$ s duration, 10 mA) delivered at 200 Hz via a bipolar electrode (PI2CEA3 concentric bipolar electrode, tip diameter 2-3  $\mu$ m platinum/iridium, Science Products GmbH) via a stimulus isolation unit

(SIU202, Warner Instruments) with a fibre optic converter (SIU202, 5V input, Warner Instruments) generated using a digitizer (Digidata 1440 series) and the clampex software (10.5.09, Molecular Devices LLC). The bipolar electrode was placed in the molecular layer of the cerebellum. Trains of 20 pulses were applied every 10 seconds over a time period of 60 seconds. After electrical stimulation, the same region of the acute slice with the same cells was recorded again.

## **4.9 Determination of protein expression levels**

To quantify relative protein expression levels, western blots were performed from cerebellar lysates.

### **4.9.1 Protein extraction**

For protein extraction, 5 animals per genotype of the same age were used. The brains were prepared as described before for slice preparation (chapter 4.2.6). The whole cerebelli were separated from the brain and frozen in liquid nitrogen.

Cerebelli were homogenized using a homogenizer containing ice cold lysis buffer in a cold room at 4° C until all pieces of tissue were in solution. The homogenate was centrifuged at 3000 g for 5 min, at 4° C to get rid of the debris. The supernatant was centrifuged at 100,000 g for 45 min, at 4° C. The supernatant containing the cytosolic protein was collected; the pellet containing the total crude membrane was resuspended in solubilizing buffer.

### **4.9.2 Determination of protein concentration**

The protein concentration was determined with a BCA assay (high range). The extinction of a 1:10 dilution of the raw protein lysate in comparison to a BSA protein standard (0, 0.5, 1, 1.5, 2 µg/µl) was measured on a NanoDrop 2000 (Thermo Scientific, Absorption at 280 nm) using the software version 1.4.2. Dilution of raw protein lysate was performed in the corresponding buffer, supplemented with Pierce BCA Protein Reagent (Thermo Scientific) and incubated for 5 min at 60° C before measurement.

### 4.9.3 SDS-PAGE

Western blots were performed using the BioRad gel system with a 12% separation gel and a 4% stacking gel. The cytosolic protein (40 µg) and the membrane protein (60 µg) were loaded with 5 x SDS sample buffer onto the SDS gel, as well as 4 µl of the dual color marker (BioRad 104-0374). The gel ran for 70 min and 200 V at room temperature. Afterwards, the gel was adjusted to the transfer buffer together with the membrane (GE Healthcare Amersham™ Hybond™ ECL) for 10 min at room temperature.

### 4.9.4 Western blot

The gel was placed on the membrane and wet plotted for 16 hours with 30 V in the cool room at 4°C with transfer buffer of pH 9.9 for EAAT1/GLAST and EAAT2/GLT1, and pH 8.0 for actin controls (using the BioRad wet blot system).

### 4.9.5 Immunodetection of proteins

The membrane was blocked for 1 h with 3% BSA (TBS) at room temperature under gentle shaking. Under permanent shaking at room temperature the membrane was incubated with the primary antibody for 1 h. Afterwards, the membrane was washed three times for 10 minutes with PBS buffer containing 0.1% Triton X-100, before the secondary antibody was applied for 1 h at room temperature. The membrane was washed again three times for 10 min with PBS/0.1% Triton X-100 and one time with PBS. Until chemiluminescence imaging the membrane was kept in PBS.

Table 4.4: **Antibodies used for immunodetection of EAAT1/GLAST, EAAT2/GLT1 and actin.**

antibodies	Dilution
anti GLAST (ms) (MACS)	1:1000
anti GLT1 (gp) (Chemicon)	1:2000
anti actin (rb) (Sigma Aldrich)	1:2000
Rabbit α mouse IgG secondary AB HRP conjugate (Pierce Thermo Scientific)	1:25000
Rabbit α guinea pig IgG secondary AB HRP conjugate (Pierce Thermo Scientific)	1:25000
Goat α rabbit IgG secondary AB HRP conjugate (Pierce Thermo Scientific)	1:25000

#### 4.9.6 Chemiluminescence imaging

Chemiluminescence imaging was performed using the GeneGnome and the software GeneSys (Syngene). The membrane was gently dried and covered with 800  $\mu$ l SuperSignal™ (Thermo Scientific).

Table 4.5: Size and isoelectric point of proteins of interest.

Protein	Size	Isoelectric point
GLAST	58 kDa	8.52
GLT1	62 kDa	6.09
Actin	42 kDa	4.8

#### 4.9.7 Blot analysis

To quantify the protein expression by western blot the software ImageJ (1.49d, Wayne Rasband, National Institutes of Health, USA) was used for band intensity analysis. The relative expression of EAAT1/GLAST and EAAT1/GLT1 was estimated by calculating the ratio between the amount of target protein and the corresponding control band of actin.

#### 4.10 Statistical analysis

The protein expression ratios were compared using a two tailed-students t-test. All chloride concentrations are given as mean values of all cells measured under the same conditions  $\pm$  95% confidence intervals. All different experimental conditions were performed on slices of at least three animals. Statistical analysis was performed by a two tailed student's t-test, or, if the values were not normally distributed, by using the Mann-Whitney Rank Sum Test. Asterisks indicate the level of significance (\*\*\*,  $p < 0.001$ ; \*\*,  $p < 0.01$ ; \*,  $p < 0.05$ ). A normal distribution of datasets was verified by Shapiro-Wilk tests. All determined values and test results are listed in table 5.1-5.6.

## 4.11 Buffer

### 4.11.1 MQAE characterization

#### Intracellular solution (IS, high chloride)

140 mM	KCl
2 mM	MgCl <sub>2</sub>
20 mM	HEPES
2 mM	Mg-ATP

pH adjusted to 7.3 with KOH.

#### Intracellular solution (IS, chloride free)

140 mM	Gluconic acid potassium salt
2 mM	MgCl <sub>2</sub>
20 mM	HEPES
2 mM	Mg-ATP

pH adjusted to 7.3 with KOH.

### 4.11.2 Primary cultured astrocytes (pc-astrocytes)

#### IP-astrocytes base media

50%	Neurobasal medium (Gibco)
50%	DMEM (Invitrogen)
100 units	Penicillin
100 µg/ml	Streptomycin
1 mM	Sodium Pyruvate
292 µg/ml	l-glutamine
1x	SATO
5 µg/ml	N-acetyl-L-cysteine

**SATO (100x)**

100 µg/ml	Transferrin
100 µg/ml	Bovine serum albumin
16 µg/ml	Putrescine
0.2 µM	Progesterone
add	Neurobasal medium

**MD-astrocytes growth media**

86%	DMEM
10%	Fetal calf serum
5 ml	Penicillin-streptomycin
2 mM	Glutamine
1 mM	Sodium pyruvate
5 µg/ml	Insulin
5 µg/ml	N-acetyl-L-cysteine
10 µM	Hydrocortisone

**4.11.3 Acute cerebellar slices****Ringer's solution (10x)**

1250 mM	NaCl
25 mM	KCl
12,5 mM	NaH <sub>2</sub> PO <sub>4</sub>
260 mM	NaHCO <sub>3</sub>

Filtered and stored at 4°C.

**Normal Ringer's solution**

2 mM	CaCl <sub>2</sub>
1 mM	MgCl <sub>2</sub>
10 v/v	10 x Ringer's solution

10 mM	D-glucose
-------	-----------

#### Preparation Ringer's solution

0.5 mM	CaCl <sub>2</sub>
5 mM	MgCl <sub>2</sub>
10 v/v	10 x Ringer's solution
25 mM	D-glucose

#### KCl-buffer

140 mM	KCl
10 mM	HEPES
10 mM	Gluconic acid sodium salt

Osmolarity adjusted to 310 mOsm, pH adjusted to 7.4 with KOH and stored at 4 °C.

#### K-gluc-buffer

140 mM	Gluconic acid potassium salt
10 mM	HEPES
10 mM	Gluconic acid sodium salt

Osmolarity adjusted to 310 mOsm, pH adjusted to 7.4 with KOH and stored at 4 °C.

#### 4.11.4 Protein quantification

##### Separation gel (12%)

0.375 M	Tris-HCl, pH 8.8
0.1%	Sodium dodecyl sulfate (SDS)
12%	Acrylamide bis solution
0.1%	Ammonium persulfate (APS)
0.1%	TEMED

**Stacking gel (4%)**

0.25 M	Tris-HCl, pH 6.8
0.1%	SDS
4%	Acrylamide bis solution
0.05%	APS
0.1%	TEMED

**Phosphate buffered saline (PBS)**

140 mM	NaCl
2.7 mM	KCl
10 mM	NaH <sub>2</sub> PO <sub>4</sub>
1.8 mM	KH <sub>2</sub> PO <sub>4</sub>

**Tris buffered saline (TBS)**

10 mM	Tris
150 mM	NaCl

**Transfer buffer**

10 mM	NaHCO <sub>3</sub>
3 mM	Na <sub>2</sub> CO <sub>3</sub>

pH adjusted to 9.9 or 8.0 with NaOH, respectively.

**SDS sample buffer (5x)**

300 mM	Tris
10%	SDS
50%	Glycerol
50 mM	DTT
0.05%	Bromophenol blue

**SDS running buffer, pH 8.3**

25 mM	Tris
192 mM	Glycine
0.1%	SDS

**Lysis buffer**

1 mM	EDTA
10 mM	Tris-Cl, pH 7.4
0.1 mM	DTT
2 µl/ml	Protease inhibitor cocktail

**Solubilizing buffer**

1 mM	EDTA
50 mM	Tris-Cl, pH 7.4
1% (v/v)	Triton X-100
0.5% (w/v)	SDS
2 µl/ml	Protease inhibitor cocktail

## 5 Results

### 5.1 Determination of $[Cl^-]_{int}$ in primary astrocytic cell culture

Primary culture of EAAT1/GLAST expressing astrocytes as a model for cerebellar Bergmann glia was used for in vitro calibration of MQAE with the two-ionophore method. After 5 to 26 days in vitro (DIV), glial cells appear in different shapes, and one example for fluorescence intensity and the corresponding fluorescence lifetime image of pc-astrocytes is shown in figure 5.1. The intensity image demonstrates that the soma and thin fibres are efficiently loaded with MQAE. The corresponding fluorescence lifetime image shows the average fluorescence lifetime for these cells, represented by a colour code.

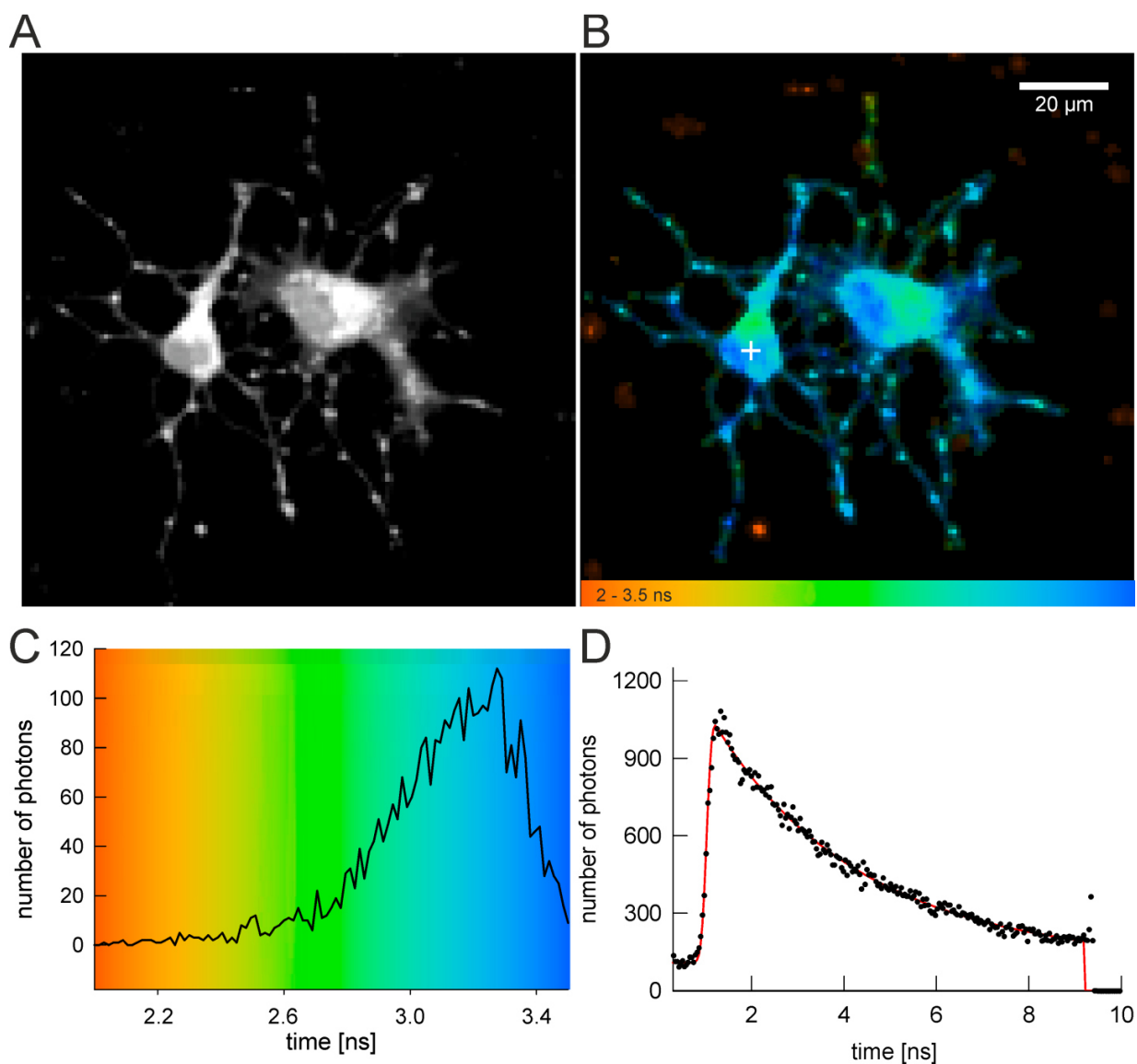


Figure 5.1: **Fluorescent intensity and fluorescence lifetime image of MQAE loaded pc-astrocytes.** A: Fluorescent intensity image of MQAE loaded pc-astrocytes. B: Corresponding fluorescence lifetime image showing the average fluorescence lifetime, represented through a colour code (2 – 3.5 ns). C: Distribution of the average fluorescence lifetimes of the pixels in B. D: The fluorescence decay of the pixel shown in B (white cross), the red curve represents the bi-exponential fit curve, the average fluorescence lifetime for this pixel is 3.34 ns.

The chloride dependence of MQAE fluorescence lifetime in pc-astrocytes was determined by calibration using the two-ionophore method. For each different chloride concentration (4, 20, 40, 60, 80 and, 100 mM) around ten cells were calibrated and the average fluorescence lifetime

of the soma was determined. The existence of subpopulations among pc-astrocytes, as indicated by differences in size or shape, was neglected for the calibration. During calibration, when chloride concentrations were clamped from 100 to 4 mM, the fluorescence lifetime changes from 2 to 3.5 ns. This change is indicated in figure 5.2 by a colour switch from red to orange and blue.

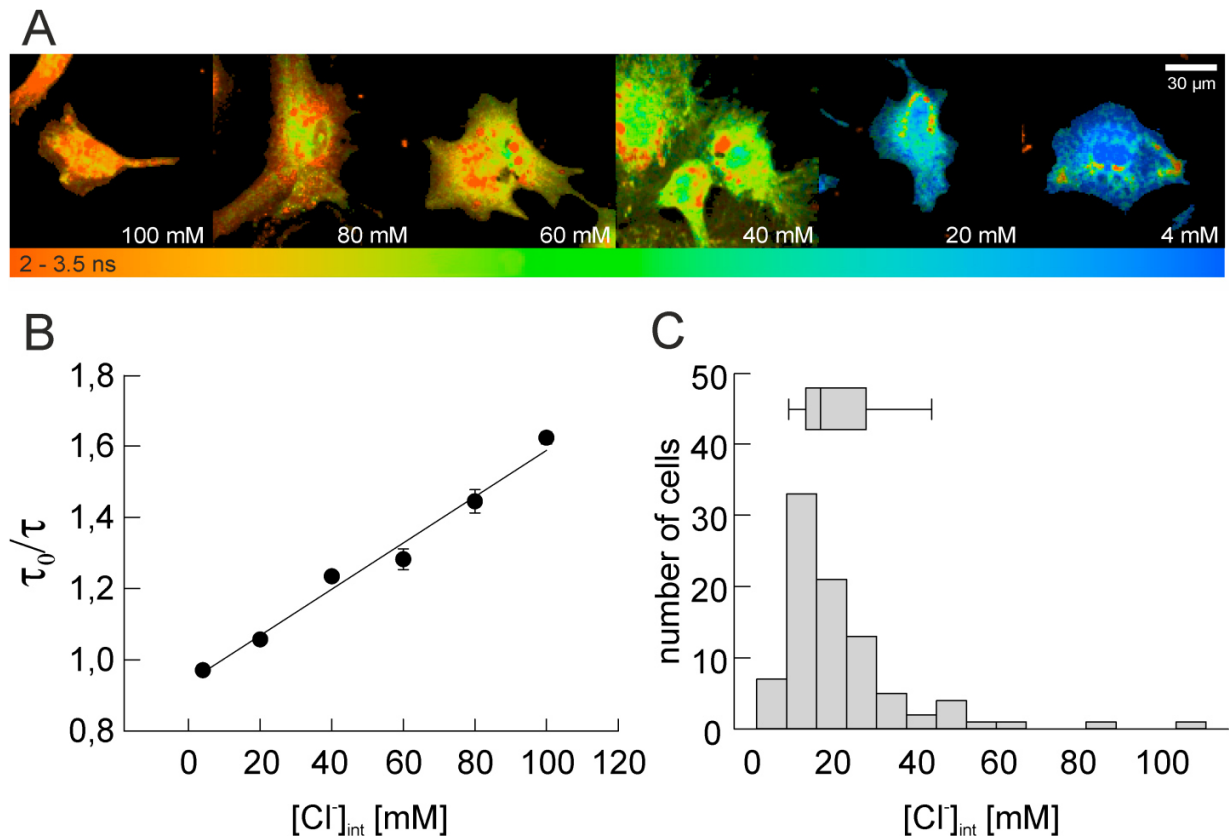


Figure 5.2: **Calibration and determination of the [Cl<sup>-</sup>]<sub>int</sub> of pc-astrocytes.** By use of the two-ionophore method the fluorescence lifetime of MQAE was calibrated for different chloride concentrations. A: Fluorescence lifetime images of different pc-astrocytes during the calibration of fluorescence lifetime of MQAE for chloride. The different intracellular chloride concentrations applied, result in different average fluorescence lifetimes, represented by different colours (2 - 3.5 ns). B: The fluorescence lifetime of MQAE for 4 to 100 mM [Cl<sup>-</sup>]<sub>int</sub> was measured and the Stern-Volmer plot was generated, the  $K_{SV}$  is  $6.6 \text{ M}^{-1}$  ( $R^2 = 0.89$ ). C: Distribution of the [Cl<sup>-</sup>]<sub>int</sub> of 89 pc-astrocytes after 5 to 26 (DIV). The mean value is  $22.8 \pm 16.7 \text{ mM}$  (SD).

To calculate the Stern-Volmer constant, the inverse fluorescence lifetime normalized to the inverse fluorescence lifetime at 4 mM, was plotted and a linear regression curve was calculated. The resulting  $K_{SV}$  is  $6.6 \text{ M}^{-1}$  ( $R^2 = 0.98$ ). This calibration curve was used to determine the average

$[Cl^-]_{int}$  of pc-astrocytes of all different shapes. The distribution in figure 5.2 shows the  $[Cl^-]_{int}$  of 89 pc-astrocytes after 5 to 26 (DIV) and is asymmetrically shaped and not normally distributed ( $W = 0.765$ ,  $p < 0.001$ ). Most cells show lower, whereas only a few cells show higher chloride concentrations. The mean value is  $22.8 \pm 16.7$  mM (SD), and the median is 17.4 mM. The  $[Cl^-]_{int}$  of 80% of the cells, which have  $[Cl^-]_{int}$  in the central region symmetrically around the median, fall into the range of 9.7 to 44.4 mM. The distribution of the intracellular chloride concentration shows a broad range, however, the values are consistent with chloride concentrations determined with other methods before, ranging from 20 to 55 mM (Bekar and Walz, 2002, Kimelberg, 1981, Kimelberg et al., 1979, Walz and Hertz, 1983, Kettenmann et al., 1987). The calculated calibration curve shows a high determination coefficient ( $R^2 = 0.98$ ) indicating, that EAAT1/GLAST expressing glial cells can be calibrated using the two-ionophore method.

## 5.2 Determination of the $[Cl^-]_{int}$ in Bergmann glia of acute cerebellar slices

### 5.2.1 FLIM imaging in Bergmann glia of acute cerebellar slices

To investigate the function and properties of Bergmann glia in their physiological environment, FLIM experiments of MQAE-loaded acute cerebellar slices from mice were used to monitor the  $[Cl^-]_{int}$  of Bergmann glia at rest and different stimuli as well as pharmacological treatment. A representative FLIM measurement of a MQAE loaded acute cerebellar slice is shown in figure 5.3. The image on the left shows the fluorescence intensity of MQAE. The structure of the cerebellar cortex, consisting of three layers is recognisable. These layers are the granule cell layer, the Purkinje cell layer, harbouring Purkinje neurons as well as Bergmann glia, and the molecular layer. Due to their characteristic morphology, size, and location, the somata of Bergmann glia can be identified in the Purkinje cell layer between the Purkinje neurons. Their fibres, reaching outwards through the molecular layer towards the *pia mater*, are visible as well. Bergmann glia somata are sufficiently loaded with MQAE, and show higher fluorescence intensity compared to the surrounding cells, which show much lower MQAE accumulation. The

corresponding FLIM image on the right (Fig. 5.3 B) shows the calculated average fluorescence lifetime represented through the colour code (3.5 – 5 ns).

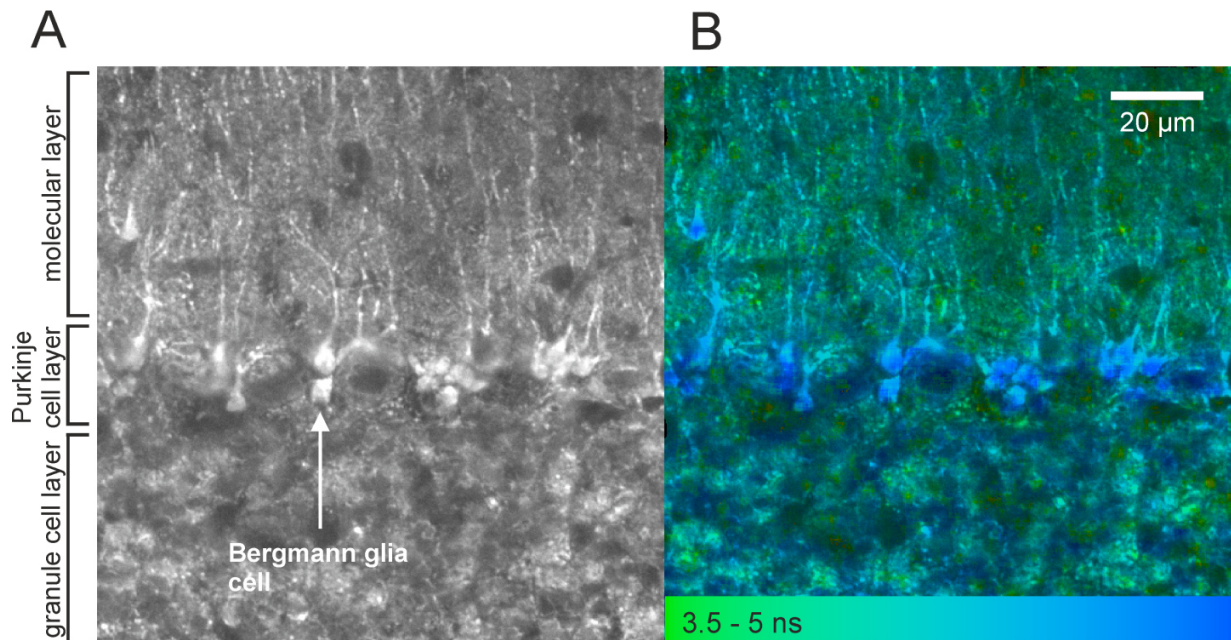


Figure 5.3: **Fluorescence intensity and fluorescence lifetime image of a MQAE loaded acute cerebellar slice.** A: Fluorescence intensity image of a MQAE loaded acute cerebellar slice. B: Corresponding fluorescence intensity image showing the average fluorescence lifetime, represented by a colour code (3.5 - 5 ns). In both images, the structure of the cerebellar cortex is recognisable. Bergmann glial cells are located in the Purkinje cell layer and one representative cell is indicated by an arrow.

The fluorescence lifetime of MQAE in Bergmann glial cells of acute cerebellar slices was calibrated as described before for pc-astrocytes (chapter 4.6.1). The fluorescence lifetime for different chloride concentrations in Bergmann glia was determined and the Stern-Volmer plot was generated (Fig. 5.4) by plotting the inverse fluorescence lifetime against the chloride concentration and fitting a linear regression curve ( $R^2 = 0.94$ ). The resulting Stern-Volmer constant in Bergmann glial cells is  $17 \text{ M}^{-1}$  and thus, significantly different from pc-astrocytes.

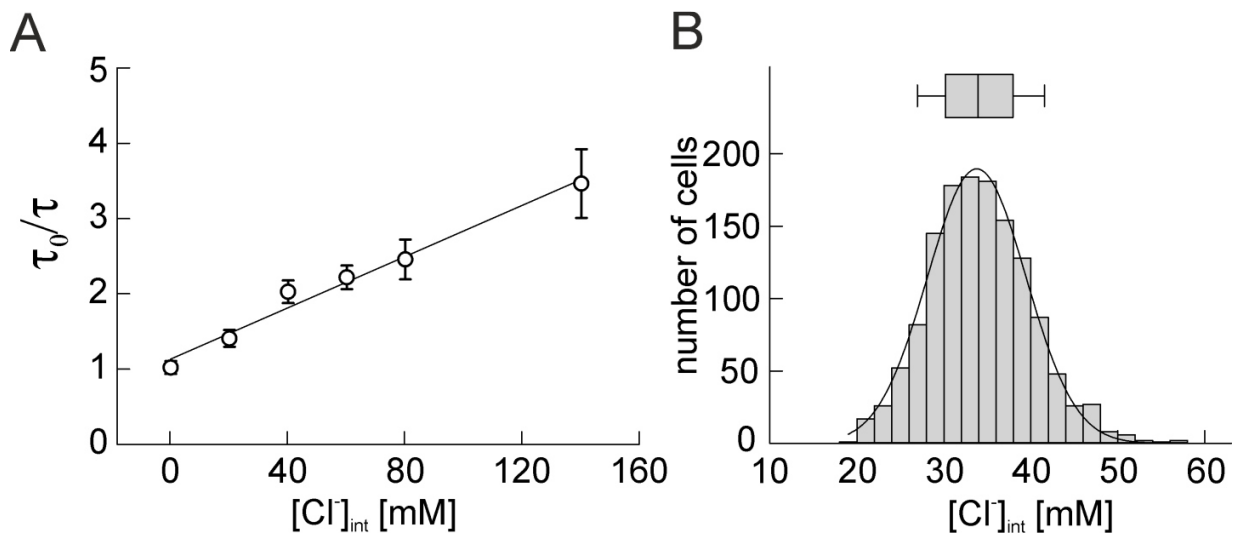


Figure 5.4: **Calibration of the fluorescence lifetime of MQAE and determination of the  $[Cl^-]_{int}$  in Bergmann glia of acute cerebellar slices.** A: Using the two ionophore method different chloride concentrations were calibrated and the corresponding Stern-Volmer plot was generated, the resulting  $K_{SV}$  is  $17 \text{ M}^{-1}$  ( $R^2 = 0.935$ ). B: Distribution of  $[Cl^-]_{int}$  of 1355 Bergmann glia measured in 84 acute cerebellar slices from 33 animals (P20 - P100). The mean value is  $34.2 \pm 5.8 \text{ mM}$  (SD) and the median is  $33.9 \text{ mM}$ .

Figure 5.4 represents the distribution of 1355 Bergmann glial cells measured in 84 acute cerebellar slices from 33 animals P20-100. The distribution is not normal distributed ( $W = 0.992$ ,  $p < 0.001$ ) with a mean value of  $34.2 \pm 5.8 \text{ mM}$  (SD) while the median amounts to  $33.9 \text{ mM}$ . Glial  $[Cl^-]_{int}$  is well above the diffusion equilibrium indicating that Bergmann glia actively accumulate chloride. The intracellular chloride concentrations of pc-astrocytes and Bergmann glia in acute cerebellar slices are significantly different ( $p < 0.001$ , Mann-Whitney Rank Sum Test). This could be an effect of changes on properties of pc-astrocytes.

### 5.2.2 The role of cation chloride cotransporters in chloride homeostasis of Bergmann glia

If chloride were to be passively distributed in glia,  $[Cl^-]_{int}$  values close to the potassium reversal potential of around  $8 \text{ mM}$  would be expected. For Bergmann glia it was demonstrated in the previous chapter, that the  $[Cl^-]_{int}$  is much higher than the diffusion equilibrium. To obtain  $[Cl^-]_{int}$  of around  $34 \text{ mM}$ , Bergmann glia need to actively accumulate chloride. Cation chloride cotransporters are chloride im- or exporters, known to set  $[Cl^-]_{int}$  in neurons (Rivera et al., 1999).

Three of them are expressed in Bergmann glia as well. These are the chloride importer NKCC1, and the chloride exporter KCC1 and KCC3. To test the influence of NKCC1 on the  $[Cl^-]_{int}$  of Bergmann glia, acute cerebellar slices were incubated with 40  $\mu$ M Bumetanide, which specifically blocks NKCC1 (Payne et al., 2003), and  $[Cl^-]_{int}$  was measured using FLIM. Figure 5.5 shows an example for a MQAE loaded slice incubated with Bumetanide. In this close up of the Purkinje cell layer, Bergmann glia somata (an example is marked by a white arrow) become visible. Their fibres reach outwards, here upwards through the molecular layer, while the granule cell layer is located below. The fluorescence lifetime represented through a colour code (3.5 – 5 ns) shows a darker blue in Bergmann glia somata representing longer fluorescence lifetimes compared to measurements under physiological conditions.

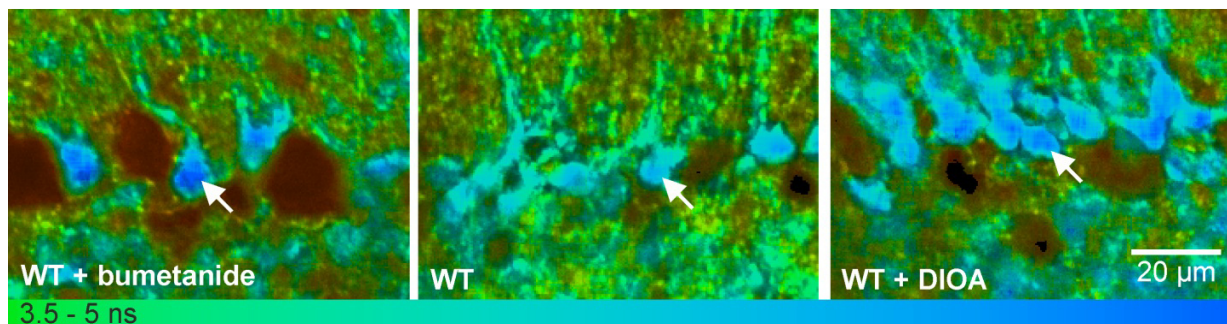


Figure 5.5: **Fluorescence lifetime image of an acute cerebellar slice incubated with Bumetanide or DIOA, respectively.** FLIM image of an acute cerebellar slice 10 min after the application of 40  $\mu$ M Bumetanide to specifically block NKCC1 (left), under physiological conditions (middle) and 20 min after the application of 80  $\mu$ M DIOA to block KCC1 and 3 (right), respectively. One Bergmann glia soma is marked by an arrow in every close up of the Purkinje cell layer.

The effect of Bumetanide was measured for 221 cells in 9 acute cerebellar slices from 3 animals (P20) and is shown in figure 5.6. 10 min after the application of Bumetanide, the  $[Cl^-]_{int}$  amounts to  $28.5 \pm 5.6$  mM (mean  $\pm$  SD), the median is 28.2 mM. This significant decrease in intracellular chloride concentrations shows that NKCC1 plays a role in chloride accumulation in Bergmann glia. The value is still above the diffusion equilibrium, indicating that other proteins are involved in chloride accumulation. A corresponding effect on intracellular sodium concentrations upon Bumetanide application were observed by Niklas J. Gerkauf and Christine R. Rose, Institute of Neurobiology, Düsseldorf (Untiet et al., 2016). A similar decrease in  $[Na^+]_{int}$  of around 6 mM was measured (Untiet et al., 2016).

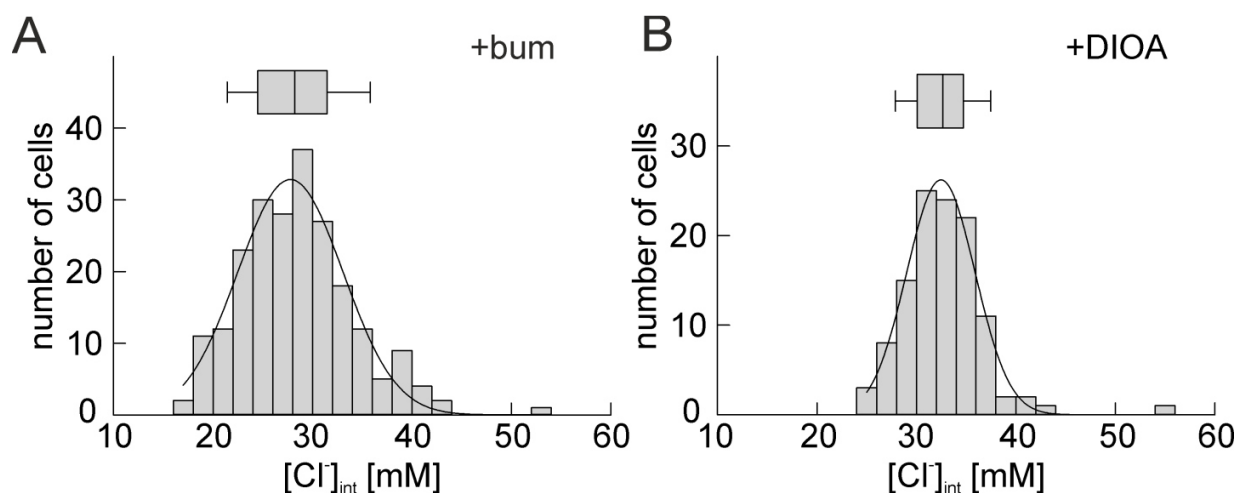


Figure 5.6: **The  $[Cl^-]_{int}$  in acute cerebellar slices incubated with Bumetanide or DIOA, respectively.** A: Distribution of the  $[Cl^-]_{int}$  of 221 Bergmann glia measured in 9 acute cerebellar slices from 3 animals (P20) 10 min after the application of 40  $\mu$ M Bumetanide. The mean value is  $28.5 \pm 5.6$  mM (SD), and the median 28.2 mM. The population is not normally distributed ( $W = 0.976$ ,  $p < 0.001$ , Shapiro-Wilk). B: Distribution of the  $[Cl^-]_{int}$  of 114 Bergmann glia measured in 5 acute cerebellar slices from 3 animals (P20) 20 min after the application of 80  $\mu$ M DIOA. The mean value is  $32.7 \pm 4.1$  mM (SD), the median is 32.7 mM, too.

To investigate on the role of KCC1 and KCC3, another blocker was used. Both KCCs can be blocked at comparable efficiency using DIOA (Mercado et al., 2000). An example for a MQAE loaded acute cerebellar slice, after the incubation with 80  $\mu$ M DIOA for 20 min, is shown in figure 5.5. The slice shows the same orientation as described before, however, the fluorescence lifetime of Bergmann glia somata is represented in lighter blue, and hereby in the same range as under physiological conditions. In total, 114 Bergmann glia in 5 slices from 3 animals (P20) were measured 20 min after the application of 80  $\mu$ M DIOA and plotted in figure 5.6. The  $[Cl^-]_{int}$  are normally distributed with a mean of  $32.7 \pm 4.1$  mM (SD) while the median is 32.7 mM. In Bergmann glia KCCs do not play a central role in chloride homeostasis, in contrast to NKCC1 (Fig. 5.7). KCC1 and KCC3 have been described to be inactive under physiological conditions (Kahle et al., 2010) thus these chloride exporter are not expected to be active and specific blocking is unlikely to have any effect as it was demonstrated here.

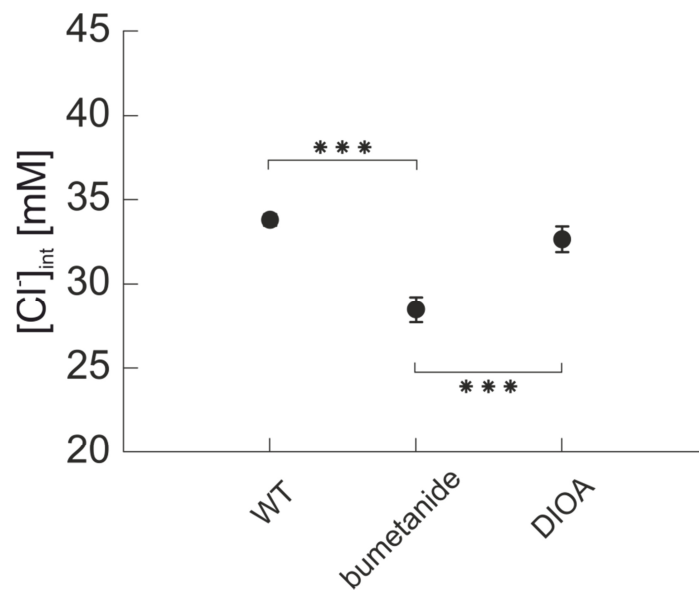


Figure 5.7: **The effect of cation-chloride-cotransporter blocker Bumetanide and DIOA on the  $[Cl^-]_{int}$  in acute cerebellar slices.** Due to the application of Bumetanide and thereby blocking NKCC1, intracellular chloride concentrations are significantly decreased ( $28.5 \pm 0.7$  mM;  $p < 0.001$ , two tailed t-test), while the application of DIOA, blocking KCC1 and KCC3, leaves  $[Cl^-]_{int}$  unaffected ( $32.7 \pm 0.8$  mM,  $p = 0.010$ , Mann-Whitney Rank Sum Test). Bergmann glia of slices incubated with Bumetanide have significantly lower chloride concentrations compared to cells of slices incubated with DIOA ( $p < 0.001$ , Mann-Whitney Rank Sum Test). All data are given as mean values  $\pm$  95% confidence intervals.

### 5.2.3 The effect of chloride channel on the $[Cl^-]_{int}$ of Bergmann glial cells

Bergmann glial cells express different types of chloride channels. These include the voltage gated chloride channel CIC-2, the excitatory amino acid transporters EAAT1/GLAST and EAAT2/GLT, and the volume-activated chloride channel VRAC and VSOC. VRAC and VSOC are activated mostly under pathological conditions (Hydzinski-Garcia et al., 2014) and for this reason not further investigated in this work.

#### 5.2.3.1 The voltage gated chloride channel CIC-2 does not affect the intracellular chloride in Bergmann glia

The voltage dependent chloride channel CIC-2 (*Clcn2*) opens below the negative resting potential, and is activated during cell swelling and extracellular acidification (Jordt and Jentsch, 1997). Since no specific blocker for CIC-2 is available (Zifarelli and Pusch, 2012), the CIC-2 *knock-out* mouse was used to investigate the influence of CIC-2 on the  $[Cl^-]_{int}$  of Bergmann glia. For determination of the  $[Cl^-]_{int}$  of Bergmann glia, cells of 10 acute cerebellar slices from 3 animals (P20) were measured, under physiological conditions. Since CIC-2 animals show a vacuolation phenotype in older animals (Blanz et al., 2007) the measurements were restricted on animals at the age of P20. The  $[Cl^-]_{int}$  of 148 cells were plotted in figure 5.8. The histogram is normally distributed ( $W = 0.989$ ,  $p = 0.324$ , Shapiro-Wilk) with a mean of  $33.2 \pm 3.7$  mM (SD), the median is 32.5 mM. Due to its properties and its severe phenotype it is surprising that the deletion of CIC-2 leaves the intracellular chloride concentration of Bergmann glia unaffected. An explanation may be that due to some other channel activating processes in Bergmann glia, the channel has no effect under physiological conditions. At the same time these results explain why next to retinal degeneration and male infertility the *Clcn2*<sup>-/-</sup> do not have an astrocytic phenotype.

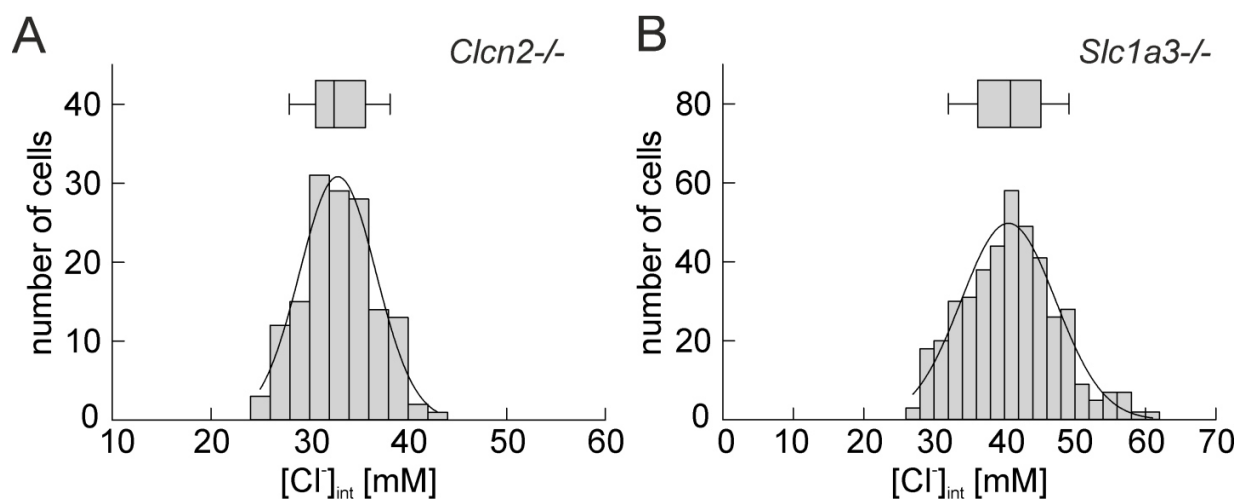


Figure 5.8: **The  $[Cl^-]_{int}$  in Bergmann glia of acute cerebellar slices of *Clcn2*<sup>-/-</sup> and *Slc1a3*<sup>-/-</sup> mice.** A: Distribution of the  $[Cl^-]_{int}$  of 148 Bergmann glia measured in 10 acute cerebellar slices from 3 animals (P20) of *Clcn2*<sup>-/-</sup> mice under physiological conditions. The mean value is  $33.2 \pm 3.7$  mM (SD) the median is 32.5 mM. The population is not normally distributed ( $W = 0.989$ ,  $p = 0.324$ , Shapiro-Wilk). B: Distribution of the  $[Cl^-]_{int}$  of 418 Bergmann glia measured in 40 acute cerebellar slices from 17 animals (P20-100) of *Slc1a3*<sup>-/-</sup> mice under physiological conditions. The population is not normally distributed ( $W = 0.988$ ,  $p = 0.002$ , Shapiro-Wilk). The mean  $[Cl^-]_{int}$  is  $38.8 \pm 6.5$  mM (SD), the median is 39.1 mM.

### 5.2.3.2 EAAT1/GLAST directly affects intracellular the chloride concentrations in Bergmann glia

Another class of glial chloride channels belongs to the solute carrier 1 family. Mouse Bergmann glia express two members of this family, EAAT1/GLAST (*Slc1a3*) and EAAT2/GLT1 (*Slc1a2*) (Grewer et al., 2014). EAATs are dual function proteins, besides their glutamate transport function, they are anion channels as well. Considering the properties of glial cells in accumulation of intracellular chloride, the opening of EAAT anion channels will lead to chloride effluxes. To investigate the influence of EAATs on the  $[Cl^-]_{int}$  of glial cells, chloride concentrations in EAAT1/GLAST *knock-out* animals (*Slc1a3*<sup>-/-</sup>) (Watase et al., 1998) were studied. The  $[Cl^-]_{int}$  of 418 Bergmann glia in 40 slices from 17 *Slc1a3*<sup>-/-</sup> mice were measured and plotted in figure 5.8. These values are not normally distributed ( $W = 0.988$ ,  $p = 0.002$ , Shapiro-Wilk). They show an average  $[Cl^-]_{int}$  of  $40.9 \pm 6.9$  mM (SD) and a median of 40.8 mM. The  $[Cl^-]_{int}$  in Bergmann glia of *Slc1a3*<sup>-/-</sup> are higher compared to wild type ( $p < 0.001$ , Mann-Whitney Test). These results show, that the function of the EAAT1/GLAST anion channel effects the  $[Cl^-]_{int}$ . The missing effect on

$[Cl^-]_{int}$  in *Cln2*<sup>-/-</sup> underlines the importance of EAAT1/GLAST anion channels which significantly change the  $[Cl^-]_{int}$  in Bergmann glia.

### **5.3.2.3 Pharmacological blocking revealed a cellular role of EAAT1/GLAST and EAAT2/GLT1 on the $[Cl^-]_{int}$ of Bergmann glia**

To confirm that the increase in  $[Cl^-]_{int}$  is due to EAAT1/GLAST and not caused by changes in protein expression levels, specific blockers were applied on acute cerebellar slices from wild type and *Slc1a3*<sup>-/-</sup> animals. UCPH-101 is a highly specific EAAT1/GLAST blocker, and incubation of acute cerebellar slices resulted in an increase of the  $[Cl^-]_{int}$  to a value of  $43.1 \pm 1.0$  mM (95% CI), while no notable changes could be determined in *Slc1a3*<sup>-/-</sup> upon application of UCPH-101. Chloride concentrations are increasing even above the value determined in *Slc1a3*<sup>-/-</sup> Bergmann glia. To investigate if EAAT2/GLT1 influences the  $[Cl^-]_{int}$  as well, and if it is upregulated in *Slc1a3*<sup>-/-</sup>, EAAT1/GLAST and EAAT2/GLT1 were simultaneously blocked using 100  $\mu$ M DL-TBOA. DL-TBOA is a general EAAT blocker, with a higher affinity for EAAT2/GLT1 than for EAAT1/GLAST (Shimamoto et al., 1998). Intracellular chloride concentration of wild type and *Slc1a3*<sup>-/-</sup> were measured while simultaneously blocking of EAAT1/GLAST and EAAT2/GLT1. In the case of wild type, as well as in the case of *Slc1a3*<sup>-/-</sup>, the  $[Cl^-]_{int}$  are increased to the same level of  $50.1 \pm 2.1$  mM (95% CI) for WT, and  $51.4 \pm 1.5$  mM (95% CI) for *Slc1a3*<sup>-/-</sup> (Fig. 5.9).

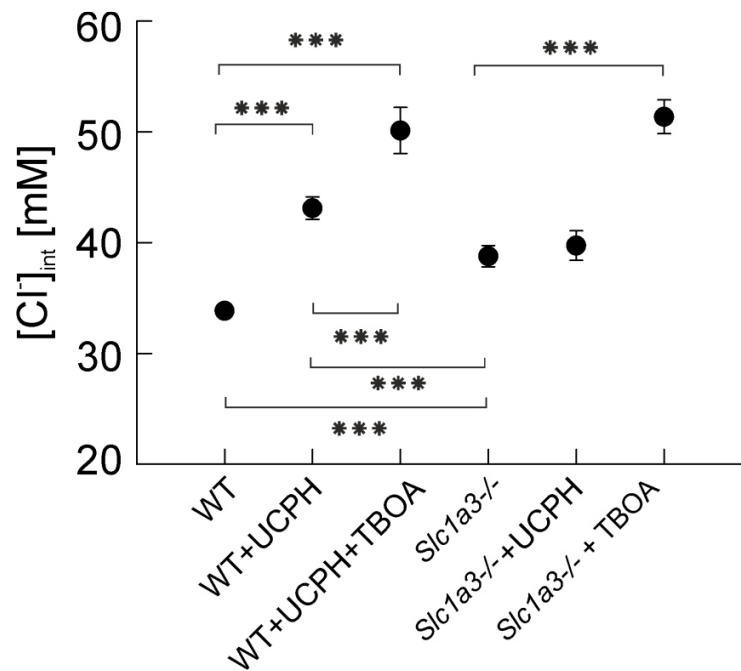


Figure 5.9: **Blocking EAAT1/GLAST and EAAT2/GLT1 directly affects the  $[Cl^-]_{int}$  of Bergmann glia in acute cerebellar slices.** The  $[Cl^-]_{int}$  in *Slc1a3*<sup>-/-</sup> is significantly higher compared to WT ( $p < 0.001$ , Mann-Whitney Rank Sum Test), blocking EAAT1/GLAST using UCPH-101 results in a significant increase of  $[Cl^-]_{int}$  compared to WT ( $p < 0.001$ , Mann-Whitney Rank Sum Test) as well as *Slc1a3*<sup>-/-</sup> ( $p < 0.001$ , Mann-Whitney Rank Sum Test), whereas application of UCPH-101 leaves the  $[Cl^-]_{int}$  in *Slc1a3*<sup>-/-</sup> unaffected ( $p = 0.250$ , Mann-Whitney Rank Sum Test). Simultaneously blocking of EAAT1/GLAST using UCPH-101 and EAAT2/GLT1 using DL-TBOA leads to the same significant increase in wild type ( $p < 0.001$ , Mann-Whitney Rank Sum Test) and *Slc1a3*<sup>-/-</sup> ( $p < 0.001$ , Mann-Whitney Rank Sum Test) compared to measurements under physiological conditions. All data are given as mean values  $\pm$  95% confidence intervals.

The expression rate of EAAT1/GLAST in the cerebellum of adult mice is six times higher compared to EAAT2/GLT1 expression (Lehre and Danbolt, 1998).  $[Cl^-]_{int}$  in Bergmann glia of *Slc1a3*<sup>-/-</sup> is significantly lower compared to wild type after application of UCPH-101. This difference could be caused by an upregulation of EAAT2/GLT1 expression levels in the EAAT1/GLAST *knock-out* animals, to compensate the loss of EAAT1/GLAST anion channels. The expression of EAAT1/GLAST and EAAT2/GLT1 was determined in wild type and *Slc1a3*<sup>-/-</sup> by western blotting and evaluated in comparison to actin expression. Figure 5.10 shows an example for one out of 5 western blots that were performed for each genotype, the bar graph demonstrates the pooled values for all 5 animals, respectively.

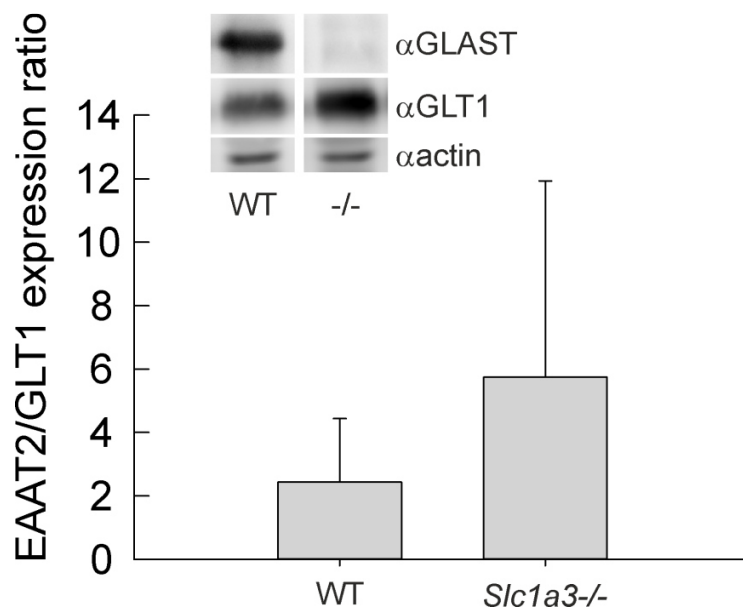


Figure 5.10: **Quantification of EAAT1/GLAST and EAAT2/GLT1 expression in the cerebellum of WT and *Slc1a3*<sup>-/-</sup> mice.** The inlay shows a representative image of a Western blot cerebellar lysate of WT and *Slc1a3*<sup>-/-</sup> incubated with  $\alpha$ GLAST,  $\alpha$ GLT1 and  $\alpha$ actin antibodies respectively. The ratio of EAAT1/GLAST to actin and EAAT2/GLT1 to actin expression is plotted, for wild type and *Slc1a3*<sup>-/-</sup>, respectively. The ratios are: WT (GLT1/actin) = 2.43; *Slc1a3*<sup>-/-</sup> (GLT1/actin) = 5.74.

The results reveal a higher value for EAAT2/GLT1 expression in the *Slc1a3*<sup>-/-</sup> compared to wild type. However this difference is not significant. Thus EAAT2/GLT1 appears not to be upregulated in EAAT1/GLAST *knock-out* animals.

#### 5.2.4 The $[Cl^-]_{int}$ in Bergmann glia changes during cerebellar development

In the rat cerebellum, as well as in other neuronal tissue, EAAT1/GLAST and EAAT2/GLT1 expression is upregulated during development (Regan et al., 2007, Schreiner et al., 2014, Ullensvang et al., 1997, Voutsinos-Porche et al., 2003, Holmseth et al., 2012). Since both glial EAATs affect the  $[Cl^-]_{int}$  of Bergmann glia it was further investigated if these chloride channels regulate the  $[Cl^-]_{int}$  in an age dependent manner. During cerebellar maturation Bergmann glia and Purkinje neurons migrate from the ventricular neuroepithelium towards the prospective cerebellar cortex. Both cell types move in two distinct layers, while Bergmann glia never overtake the Purkinje neurons. At the end of the second postnatal week, Bergmann glia form an epithelium like layer around the Purkinje neurons, which align to a monolayer. To investigate

the age-dependence of  $[Cl^-]_{int}$  in glial cells, animals from P5 to P100 were measured. Figure 5.11 shows representative FLIM images of wild type acute cerebellar slices of 5, 8 and 13 days after birth. It becomes clear that at P5 Bergmann glia and Purkinje neurons appear in two distinct layers, before they terminate their migration and build a shared layer near P13. At this point in time, migratory processes are complete (Komuro et al., 2001), and the outgrowth of fibres and dendrite trees proceeds (Yamada and Watanabe, 2002).

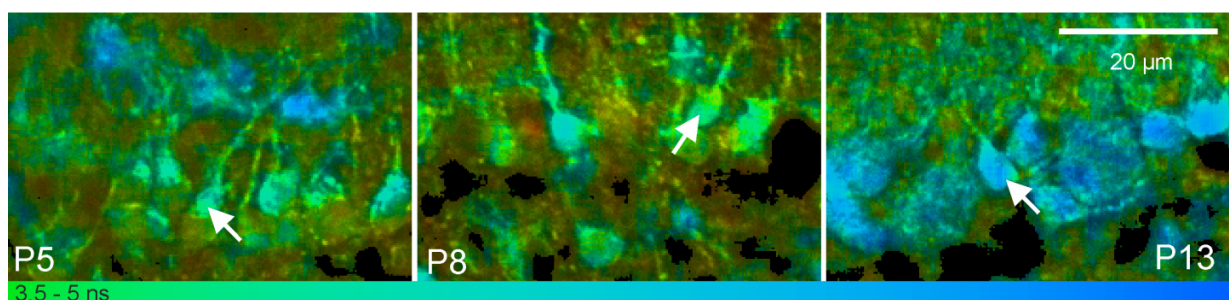


Figure 5.11: **FLIM images of acute cerebellar slices of young animals of different ages.** FLIM images of acute cerebellar slices of animals of the age of 5, 8 and 13 days after birth represent the immature structure of the cerebellar cortex, and the different chloride concentrations in Bergmann glia are shown in these states of maturation. The average fluorescence lifetime is represented through a colour code (3.5 to 5 ns). Examples of Bergmann glia are marked by white arrows.

Wild type animals of P5 and P6 show  $[Cl^-]_{int}$  of around 50 mM and a decrease upon maturation until the adult level of  $[Cl^-]_{int}$  is reached at around P13. Intracellular chloride concentrations of *Slc1a3*<sup>-/-</sup> animals from P5 to P8 are indistinguishable from wild type at P5-P6. While  $[Cl^-]_{int}$  decreases in wild type,  $[Cl^-]_{int}$  stay around 50 mM in *Slc1a3*<sup>-/-</sup> Bergmann glia at P8-9. Upon P10  $[Cl^-]_{int}$  decrease in *Slc1a3*<sup>-/-</sup> until they reach adult level, which is still significantly higher compared to wild type (Fig. 5.12). The decrease in *Slc1a3*<sup>-/-</sup> demonstrates that the chloride switch in wild type is not only caused by EAAT1/GLAST. Therefore, another chloride efflux mechanism must be involved. The dashed lines are representing the  $[Cl^-]_{int}$  upon blocking EAAT1/GLAST and EAAT2/GLT1 simultaneously in animals of age P20, which is around 50 mM. Blocker application restores the  $[Cl^-]_{int}$  of young animals (P5-6). This indicates an involvement of

both EAAT1/GLAST and EAAT2/GLT1 in the age dependent chloride switch in Bergmann glia during cerebellar maturation. To exclude the possibility that the age dependent changes in  $[Cl^-]_{int}$  are due to different properties of the fluorescence lifetime of MQAE in young animals Bergmann glia, different chloride concentrations were calibrated in younger *Slc1a3*<sup>-/-</sup> (P13) and wild type (P11), respectively (Fig. 5.12). Both values perfectly fit the calibration curve determined for wild type before.

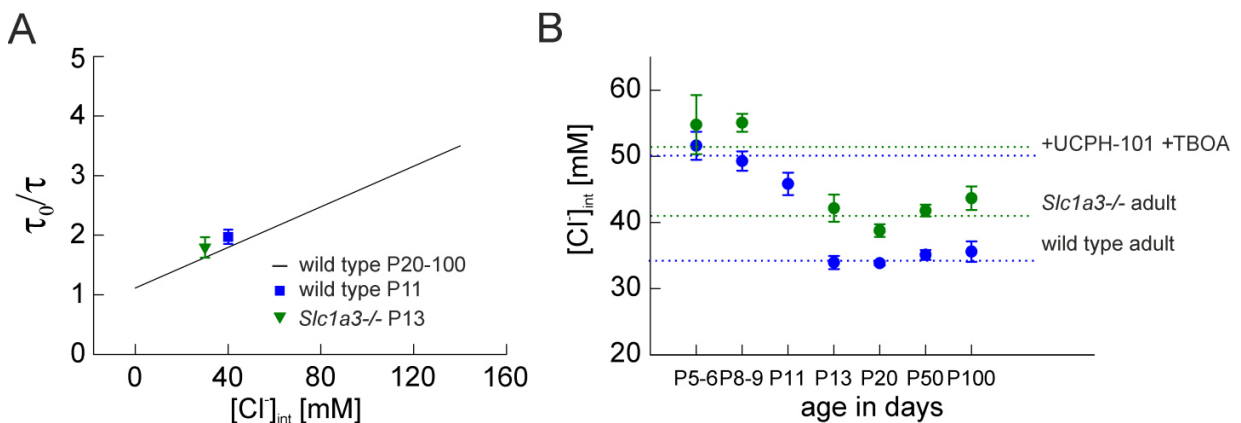


Figure 5.12: **Calibration and determination of the  $[Cl^-]_{int}$  in young animals of wild type and *Slc1a3*<sup>-/-</sup>.** A: Calibration of 30 mM chloride on Bergmann glia from *Slc1a3*<sup>-/-</sup> P13 and 40 mM in Bergmann glia from wild type P11 result in values that are in close proximity to the calibration curve determined for wild type before (chapter 5.2.1). B: The age-dependence of  $[Cl^-]_{int}$  was measured in animals at the age of 5 to 100 days after birth. Dashed lines indicate the average  $[Cl^-]_{int}$  in adult animals, and the  $[Cl^-]_{int}$  that is reached after blocking EAAT1/GLAST and EAAT2/GLT in animals of both genotypes. All data are given as mean values  $\pm$  95 % confidence intervals. (WT values are represented in blue and *Slc1a3*<sup>-/-</sup> values are shown in green).

This glial chloride switch was observed for the first time. It correlates well with the upregulation of EAAT1/GLAST and EAAT2/GLT1 expression. The neuronal chloride switch, which establishes inhibitory synaptic transmission, appears simultaneously (Rivera et al., 1999). By increasing the chloride gradient, which drives the secondary active GABA transporter, GAT, in glial cells, GABA uptake could be improved. As this glial chloride switch, glia will support inhibitory synaptic transmission to be more efficient and increase the signal to noise ratio. Furthermore, extracellular GABA levels are correlated with cell migration during cerebral maturation. The

observed glial chloride switch appears at the end of cerebellar cell migration and is correlated with the end of the developmental process.

### 5.2.5 Effects of glutamate and aspartate application on the $[Cl^-]_{int}$

It has been shown in heterologous expression systems that the EAAT anion current increases with increasing extracellular glutamate concentrations (Wadiche et al., 1995b). Thus, a dynamic adjustment of the  $[Cl^-]_{int}$  is possible as well. In order to investigate, if due to this property dynamic changes of the  $[Cl^-]_{int}$  in acute cerebellar slices are possible, high glutamate concentrations of 0.5 mM were applied on wild type and *Slc1a3*<sup>-/-</sup> slices. After 50 min of incubation with high glutamate, the  $[Cl^-]_{int}$  was decreased significantly compared to wild type under physiological conditions ( $p < 0.001$ , two tailed t-test). The average  $[Cl^-]_{int}$  decreased upon glutamate application in wild type and results in  $27.7 \pm 0.8$  mM (95% CI) whereas *Slc1a3*<sup>-/-</sup> show a much lower, non-significant decrease ( $p = 0.073$ , Mann-Whitney Rank Sum Test) to a mean value of  $37.4 \pm 2.1$  mM (95% CI) under the same conditions (Fig. 5.13).

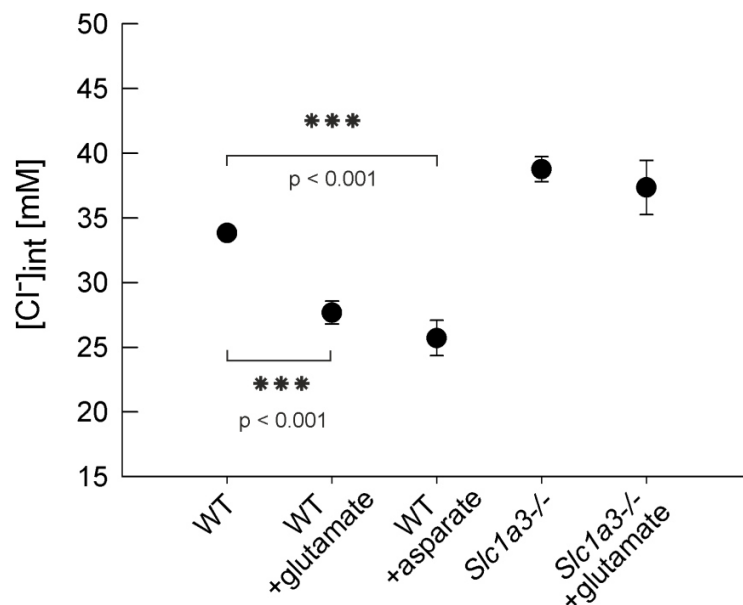


Figure 5.13: **Application of high glutamate and aspartate increase the  $[Cl^-]_{int}$  of Bergmann glia.** Application of high glutamate results in a significant decrease in the  $[Cl^-]_{int}$  of Bergmann glia of wild type ( $p < 0.001$ , Mann-Whitney Rank Sum Test). The same effect was observed after the application of aspartate ( $p < 0.001$ , Mann-Whitney Rank Sum Test). Application of glutamate on acute cerebellar slices from *Slc1a3*<sup>-/-</sup> did not change the  $[Cl^-]_{int}$  significantly ( $p=0.292$  Mann-Whitney Rank Sum Test). All data are given as mean values  $\pm$  95% confidence intervals.

To confirm that these changes in the  $[Cl^-]_{int}$  are due to glutamate binding to EAATs, resulting in a higher EAAT anion channel conductance, another substrate was applied. D-aspartate is transported by EAATs as well (Storck et al., 1992). Changing the extracellular solution to 1 mM aspartate (Bennay et al., 2008) leads to a comparable decrease of the  $[Cl^-]_{int}$ , as described above for glutamate. In total 36 cells measured in 5 slices from 3 animals showed a decreased  $[Cl^-]_{int}$  after 5 - 30 min of application, the average  $[Cl^-]_{int}$  being  $25.72 \pm 1.3$  mM (95% CI) (Fig. 5.13). Thus, it can be concluded that in the presence of a high substrate concentration, as tested here for glutamate and aspartate, the glial EAAT anion currents are increased and lead to a decrease of the  $[Cl^-]_{int}$ .

### 5.2.6 Synaptically released glutamate leads to decreased the $[Cl^-]_{int}$

Cerebellar Purkinje neurons receive excitatory input from climbing and parallel fibres, and activation of these synapses is known to activate glutamate transporters in Bergmann glia (Bergles et al., 1997, Clark and Barbour, 1997). Since high concentrations of glutamate and aspartate, as applied in chapter 5.2.5, are neurotoxic, parallel fibres were stimulated with a pulse protocol resembling physiological parallel fibre activity (van Beugen et al., 2013) to provoke synaptic release of glutamate. Electrical stimulation experiments were performed with wild type, *Slc1a3*<sup>-/-</sup>, and *Clcn2*<sup>-/-</sup> animals. Upon electrical stimulation, the  $[Cl^-]_{int}$  in wild type Bergmann glia decreased significantly. At the end of one series of stimuli the  $[Cl^-]_{int}$  was  $25 \pm 1.3$  mM (95% CI), and the same measurements in *Clcn2*<sup>-/-</sup> resulted in  $25.2 \pm 3.4$  mM (95% CI), indistinguishable from wild type. In *Slc1a3*<sup>-/-</sup> the  $[Cl^-]_{int}$  was on average  $39 \pm 2.3$  mM (95% CI) after electrical stimulation. There is no detectable difference in the  $[Cl^-]_{int}$  of *Slc1a3*<sup>-/-</sup> after electrical stimulation in comparison to the same cells under physiological conditions ( $p = 0.458$ , two tailed t-test; Fig. 5.15). Glial cells express GABA<sub>A</sub> receptors (MacVicar et al., 1989) and chloride currents due to GABA release were measured in young animals Bergmann glia (Muller et al., 1994). To confirm that the decrease in the  $[Cl^-]_{int}$  was caused by GLAST/EAAT1 and not by GABA<sub>A</sub> receptor evoked currents, the GABA<sub>A</sub> receptor blocker Bicuculline, Sigma Aldrich (Curtis et al., 1971) was applied during electrical stimulations, while the stimulation protocol remained unchanged (Bennay et al., 2008). The time responses of three single cells, of wild type with and

50

without Bicuculline, are shown in figure 5.14. Determinations of a higher temporal resolution were not possible in this approach, since every concentration determination took around 80 seconds.

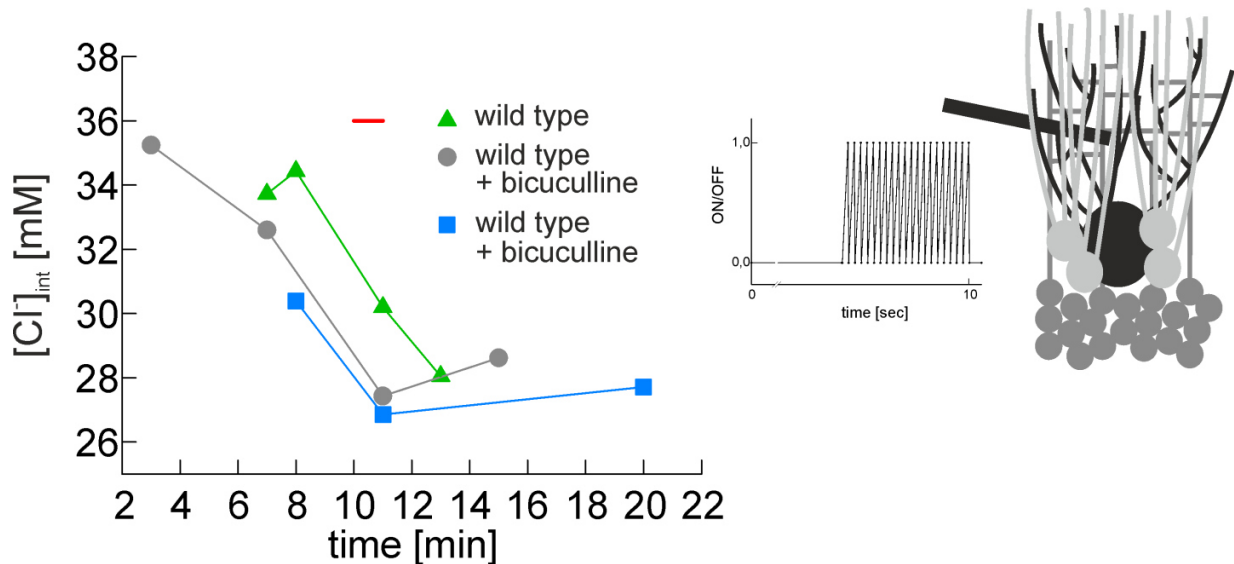


Figure 5.14: **Time dependence of the  $[Cl^-]_{int}$  upon electrical stimulation of parallel fibres.** The  $[Cl^-]_{int}$  of the same single cells before and after electrical stimulation (represented by the red line). The inlay shows a schematic illustration of the electrical stimulation protocol. Series of 20 pulses of 10 mA (150  $\mu$ s duration) at 200 Hz, via a bipolar electrode positioned within the molecular cell layer were applied. Such pulse series were repeated at a frequency of 0.1 Hz, and changes in  $[Cl^-]_{int}$  were determined by fluorescence lifetime measurements.

Measurements of 8 Bergmann glia in 4 acute cerebellar slices of 3 different animals show that  $[Cl^-]_{int}$  decreases even stronger upon electrical stimulation (Fig. 5.15). The reduction of  $[Cl^-]_{int}$  results in an average value of  $24.53 \pm 1.75$  mM (95% CI), and a median of 24.5 mM. This is significantly lower compared to values obtained before electrical stimulation in the same cells.

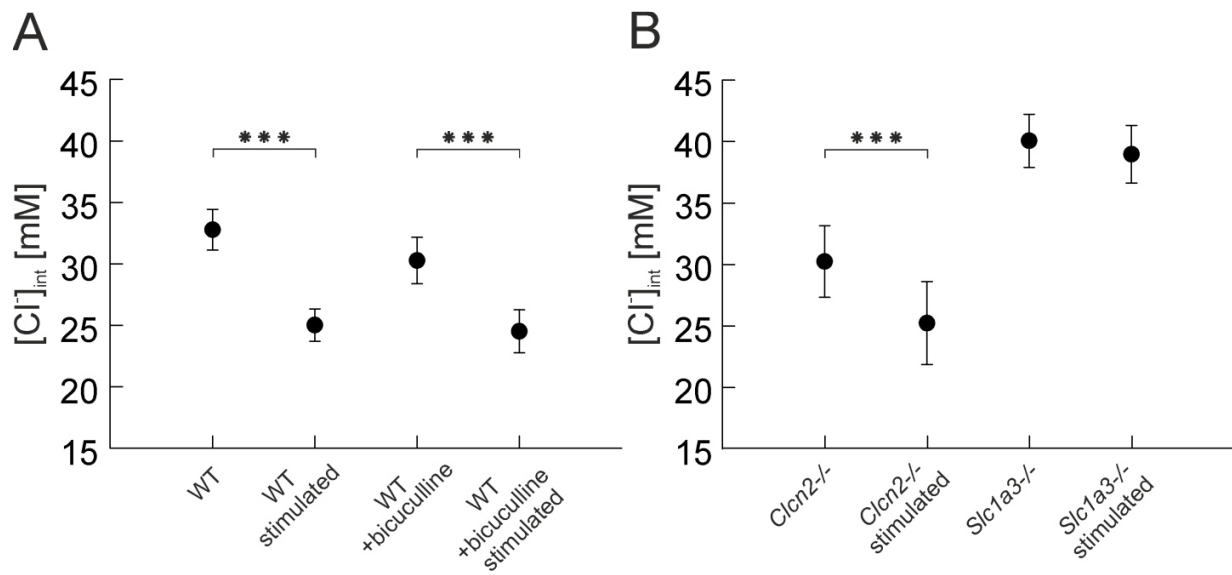


Figure 5.15: **Effect of electrical stimulation on the  $[Cl^-]_{int}$  of Bergmann glia.** A: The  $[Cl^-]_{int}$  of wild type with and without Bicuculline before and after the electrical stimulation was measured. B: The  $[Cl^-]_{int}$  of *Clcn2*<sup>-/-</sup> and *Slc1a3*<sup>-/-</sup>, before and after the electrical stimulation. All data are given as mean values  $\pm$  95% confidence interval.

### 5.3 DATA

Table 5.1: Differences between the  $[Cl^-]_{int}$  determined in different experiments and their levels of significance (\*\*\*,  $p < 0.001$ ; \*\*,  $p < 0.01$ ; \*,  $p < 0.05$ ).

Compared populations		n	Level of significance	Test
WT	pc-astrocytes	1355/89	$p < 0.001$ ***	Mann-Whitney Rank Sum Test
WT	WT + Bumetanide	993/221	$p < 0.001$ ***	Mann-Whitney Rank Sum Test
WT	WT + DIOA	993/114	$p = 0.010$ *	Mann-Whitney Rank Sum Test
WT + Bumetanide	WT + DIOA	221/114	$p < 0.001$ ***	Mann-Whitney Rank Sum Test
WT	<i>Clcn2</i> <sup>-/-</sup>	993/148	$p = 0.077$ ns	Mann-Whitney Rank Sum Test
WT	<i>Slc1a3</i> <sup>-/-</sup>	993/182	$p < 0.001$ ***	Mann-Whitney Rank Sum Test
WT	WT + UCPH	993/181	$p < 0.001$ ***	Mann-Whitney Rank Sum Test
WT	WT + UCPH + TBOA	993/63	$p < 0.001$ ***	Mann-Whitney Rank Sum Test
WT + UCPH	WT + UCPH + TBOA	181/63	$p < 0.001$ ***	Mann-Whitney Rank Sum Test
<i>Slc1a3</i> <sup>-/-</sup>	<i>Slc1a3</i> <sup>-/-</sup> + TBOA	182/93	$p < 0.001$ ***	Mann-Whitney Rank Sum Test
WT + UCPH	<i>Slc1a3</i> <sup>-/-</sup> + TBOA	181/93	$p < 0.001$ ***	Mann-Whitney Rank Sum Test
WT + UCPH + TBOA	<i>Slc1a3</i> <sup>-/-</sup> + TBOA	63/93	$p = 0.331$ ns	Two tailed Student's t-test
WT + UCPH	<i>Slc1a3</i> <sup>-/-</sup>	181/182	$p < 0.001$ ***	Mann-Whitney Rank Sum Test
<i>Slc1a3</i> <sup>-/-</sup>	<i>Slc1a3</i> <sup>-/-</sup> + UCPH	182/61	$p = 0.250$ ns	Mann-Whitney Rank Sum Test
WT P5-6	<i>Slc1a3</i> <sup>-/-</sup> P5-6	33/17	$p = 0.306$ ns	Mann-Whitney Rank Sum Test

WT P8-9	<i>Slc1a3</i> <sup>-/-</sup> P8-9	45/65	p < 0.001 ***	Mann-Whitney Rank Sum Test
WT P13	<i>Slc1a3</i> <sup>-/-</sup> P13	41/21	p < 0.001 ***	Two tailed Student's t-test
WT before stimulation	WT after stimulation	24/24	p < 0.001 ***	Two tailed Student's t-test
WT + Bicuculline before stimulation	WT + Bicuculline after stimulation	8/8	p < 0.001 ***	Two tailed Student's t-test
<i>Slc1a3</i> <sup>-/-</sup> before stimulation	<i>Slc1a3</i> <sup>-/-</sup> after stimulation	12/12	p = 0.458 ns	Two tailed Student's t-test
<i>Cln2</i> <sup>-/-</sup> before stimulation	<i>Cln2</i> <sup>-/-</sup> after stimulation	7/7	p = 0.017 *	Two tailed Student's t-test
WT after stimulation	WT + Bicuculline after stimulation	24/8	p = 0.673 ns	Two tailed Student's t-test
WT after stimulation	<i>Cln2</i> <sup>-/-</sup> after stimulation	24/7	p = 0.884 ns	Two tailed Student's t-test
WT	WT + glutamate	993/68	p < 0.001 ***	Mann-Whitney Rank Sum Test
WT	WT + aspartate	993/36	p < 0.001 ***	Mann-Whitney Rank Sum Test
<i>Slc1a3</i> <sup>-/-</sup>	<i>Slc1a3</i> <sup>-/-</sup> + glutamate	182/44	p = 0.292 ns	Mann-Whitney Rank Sum Test
Expression ratio WT	Expression ratio <i>Slc1a3</i> <sup>-/-</sup>	5/5	p = 0.114	Mann-Whitney Rank Sum Test

Table 5.2: Stern-Volmer constants ( $K_{SV}$ ) and determination coefficient ( $R^2$ ).

Cells	$K_{SV}$	$R^2$
pc-astrocytes	$6.6 \text{ M}^{-1}$	0.98
Bergmann glia	$17 \text{ M}^{-1}$	0.94

Table 5.3: Values determined for cell populations after blocker application.

Cells	age	number of cells	number of slices	number of animals	Mean	error	Median	Normally distributed	W value	P value
pc-astrocytes	DIV 5-26	89	-	-	22.8	14.7 (SD)	17.4	failed	W=0.765	p < 0.001
WT	P20-100	1355	84	33	34.2	5.8 (SD)	33.9	failed	W=0.991	p < 0.001
WT + Bumetanide	P20	221	9	3	28.5	5.6 (SD)	28.2	failed	W=0.976	p < 0.001
WT + DIOA	P20	114	5	3	32.7	4.1 (SD)	32.7	failed	W=0.905	p < 0.001
<i>Cln2</i> <sup>-/-</sup>	P20	148	10	3	33.2	3.7 (SD)	32.5	passed	W=0.989	p = 0.324
<i>Slc1a3</i> <sup>-/-</sup>	P20-100	418	40	17	40.9	6.9 (SD)	40.8	failed	W=0.988	p = 0.002
WT + UCPH	P20	181	15	5	43.1	1.0 (95% CI)	42.2	failed	W=0.959	p < 0.001
WT + UCPH + TBOA	P20	63	7	2	50.1	2.1 (95% CI)	50.0	passed	W=0.981	p = 0.433
<i>Slc1a3</i> <sup>-/-</sup> + UCPH	P20	61	4	3	39.7	1.3 (95% CI)	39.8	passed	W=0.979	p = 0.365
<i>Slc1a3</i> <sup>-/-</sup> + TBOA	P20	93	13	3	51.4	1.5 (95% CI)	50.8	passed	W=0.984	p = 0.324

Table 5.4: Values determined for different cells of animals of different ages.

Cells	age	number of cells	number of slices	number of animals	Mean	error	Median	Normally distributed	W value	P value
WT	P5-6	33	7	3	51.6	2.1 (95% CI)	49.5	passed	W=0.945	p = 0.095
WT	P8-9	45	5	2	49.3	1.5 (95% CI)	49.7	failed	W=0.922	p = 0.005
WT	P11	41	3	1	45.8	1.7 (95% CI)	46.3	passed	W=0.988	p = 9.945
WT	P13	41	2	1	33.9	1.0 (95% CI)	34.0	passed	W=0.964	p = 0.214
WT	P20	993	65	25	33.8	0.3 (95% CI)	33.8	failed	W=0.995	p = 0.002
WT	P50	303	13	5	35.1	0.7 (95% CI)	34.4	failed	W=0.985	p = 0.002
WT	P100	59	6	3	35.6	1.5 (95% CI)	36.1	passed	W=0.979	p = 0.415
<i>Slc1a3</i> <sup>-/-</sup>	P5-6	17	4	2	54.8	4.5 (95% CI)	52.1	passed	W=0.905	p = 0.082
<i>Slc1a3</i> <sup>-/-</sup>	P8-9	65	7	2	55.1	1.4 (95% CI)	54.2	passed	W=0.967	p = 0.079
<i>Slc1a3</i> <sup>-/-</sup>	P13	6	3	1	42.1	9.8 (95% CI)	42.2	passed	W=0.964	p = 0.603
<i>Slc1a3</i> <sup>-/-</sup>	P20	182	18	8	38.8	1.0 (95% CI)	39.1	failed	W=0,972	p = 0.001
<i>Slc1a3</i> <sup>-/-</sup>	P50	144	12	4	41.8	0.9 (95% CI)	41.6	passed	W=0.990	p = 0.411
<i>Slc1a3</i> <sup>-/-</sup>	P100	403	10	5	40.8	0.7 (95% CI)	43.1	passed	W=0.977	p = 0.171

Table 5.5: Values determined for cells upon substrate application or electrical stimulation, respectively.

Cells	age	number of cells	number of slices	number of animals	Mean	error	Median	Normally distributed	W value	P value
WT + glutamate	P20	68	3	3	27.4	0.8 (95% CI)	27.3	passed	W=0.989	p = 0.833
WT + aspartate	P20	36	5	3	25.72	1.3 (95% CI)	25.6	passed	W=0.953	p = 0.131
<i>Slc1a3</i> <sup>-/-</sup> +glutamate	P20	44	3	2	38.2	2.1 (95% CI)	36.9	failed	W=0.850	p < 0.001
WT before stimu	P20	24	6	4	32.8	1.7 (95% CI)	32.7	passed	W=0.969	p = 0.654
WT after stimu		24	6	4	25	1.3 (95% CI)	25.9	passed	W=0.938	p = 0.146
WT + Bicuculline before stimu	P20	8	4	3	30.3	1.9 (95% CI)	30.6	passed	W=0.907	p = 0.334
WT + Bicuculline after stimu		8	4	3	24.53	1.75 (95% CI)	24.5	passed	W=0.963	p = 0.836
<i>Slc1a3</i> <sup>-/-</sup> + stimu before	P20	12	6	3	40.1	2.2 (95% CI)	39.7	passed	W=0.932	p = 0.404
after		12	6	3	39	2.3 (95% CI)	38.5	failed	W=0.848	p = 0.034
<i>Clcn2</i> <sup>-/-</sup> before stimu	P20	7	1	1	30.2	2.9 (95% CI)	29.2	passed	W=0.899	p = 0.326
<i>Clcn2</i> <sup>-/-</sup> after stimu		7	1	1	25.2	3.4 (95% CI)	23.9	passed	W=0.865	p = 0.166

Table 5.6: Relative protein expression levels.

58

<b>Genotype</b>	<b>Expression ratio EAAT2/GLT1 vs. actin</b>	<b>SD</b>	<b>95% CI</b>
WT	2.43	1.3	2.0
<i>Slc1a3</i> <sup>-/-</sup>	5.74	4.0	6.2

## 6 Discussion

### 6.1 Intracellular chloride concentrations in cultured astrocytes

Different studies determined intracellular chloride concentrations of astrocytes. Electrophysiological approaches, for example, revealed an average  $[Cl^-]_{int}$  of 29 mM, ranging from 22 - 55 mM (Bekar and Walz, 2002). In accordance with this, radioactive chloride efflux experiments showed  $[Cl^-]_{int}$  from 31 - 50 mM (Kimelberg, 1981, Kimelberg et al., 1979, Walz and Hertz, 1983) and using  $Cl^-$  sensitive microelectrodes values between 20 - 40 mM were determined (Kettenmann et al., 1987). The  $[Cl^-]_{int}$  measured in this work in EAAT1/GLAST expressing, pc-astrocytes from whole mouse brain using FLIM and MQAE are similar to the values determined before. The average  $[Cl^-]_{int}$  is  $22.8 \pm 16.7$  mM (SD) and ranges from 14.8 to 28.5 mM. The values determined here are on the lower edge of the range of  $[Cl^-]_{int}$  described in astrocytes before, however this can be explained by the different types of astrocyte cultures used for determination. In contrast to the other studies, which used primary cultured hippocampal astrocytes (Bekar and Walz, 2002) or astrocyte cultures from the whole brain (Kettenmann et al., 1987, Kimelberg, 1981), this study used EAAT1/GLAST expressing astrocytes which were isolated and cultured. The highest  $[Cl^-]_{int}$  was determined in hippocampal astrocytes and these cells express the least amount of EAAT1/GLAST (Lehre and Danbolt, 1998). Astrocytes isolated from the whole brain, which include cerebellar astrocytes, the predominant expression site of EAAT1/GLAST, have a  $[Cl^-]_{int}$  range from 20 – 40 mM. To prepare the primary culture of EAAT1/GLAST positive astrocytes a method was used which allows only very few other cell types to be present (< 2%), for example other astrocytes or cells that do not express EAAT1/GLAST such as neurons (Foo et al., 2011). However, the chloride concentrations determined here in primary cultured astrocytes are significantly lower compared to the  $[Cl^-]_{int}$  determined in Bergmann glia from acute cerebellar slices. It is known, that glial cells are further differentiating in vitro, meaning they divide rapidly and continuously (Foo et al., 2011) and show significantly different gene expression levels (Cahoy et al., 2008, Doyle et al., 2008). Upregulation of volume regulating anion channel such as VRAC could affect  $[Cl^-]_{int}$  in cultured astrocytes (Abdullaev et al., 2006).

## 6.2 Intracellular chloride concentrations in Bergmann glia of acute cerebellar slices

Bergmann glia are the major expression site of EAAT1/GLAST and therefore FLIM was used in acute cerebellar slices to investigate the influence of EAAT1/GLAST anion channel function on the  $[Cl^-]_{int}$ . The average  $[Cl^-]_{int}$  determined in Bergmann glia is  $34.2 \pm 5.8$  mM (95%CI). This value is significantly higher compared to the value in pc-astrocytes. However, the value of the Bergmann glia population lies within the range of values determined for  $[Cl^-]_{int}$  of astrocytes before. The  $[Cl^-]_{int}$  of 34.2 mM lies well above the diffusion equilibrium and indicate that Bergmann glia actively accumulate chloride. Blocking experiments in this work demonstrated that the cation chloride cotransporter (CCC) NKCC1, plays a role in chloride accumulation in Bergmann glia, while KCC1 and KCC3 leave the  $[Cl^-]_{int}$  unaffected (Fig. 5.7). These findings are in line with the notion that KCC1 and KCC3 are not active under isosmotic conditions (Kahle et al., 2010). It has been shown that NKCC1 is constitutively active and mediates constant influx of sodium into astrocytes, as blocking NKCC1 caused a decrease in the  $[Na^+]_{int}$  in hippocampal as well as cortical astrocytes (Kelly et al., 2009, Rose and Ransom, 1996, Su et al., 2002). This effect of NKCC1 was also shown in Bergmann glia by measuring the corresponding decrease in  $[Na^+]_{int}$  by Niklas J. Gerkau and Christine R. Rose, Institute for Neuroscience, Düsseldorf (Untiet et al., 2016). Upon Bumetanide application the  $[Na^+]_{int}$  as well as the  $[Cl^-]_{int}$  decreased by around 6 mM. Due to the stoichiometric of NKCC1 transport a two times higher decrease in chloride compared to sodium is expected. In the case of chloride, the average  $[Cl^-]_{int}$  after blocker application is measured, not the time response of single cells. This allows a bigger difference to be averaged out. Furthermore, after blocking NKCC1 the  $[Cl^-]_{int}$  still lies above the diffusion equilibrium referring to other proteins that can be involved in chloride accumulation in Bergmann glia, which were not identified so far.

A combination of measuring *knock-out* animals and blocking experiments in WT demonstrated that EAAT1/GLAST and EAAT2/GLT1 directly affect  $[Cl^-]_{int}$  of Bergmann glia, while the ablation of the voltage sensitive chloride channel ClC-2 did not reveal any changes in  $[Cl^-]_{int}$  (Fig. 5.8). ClC-2 currents can be recorded from Bergmann glia in acute slices, however, these currents differ in time and voltage dependence from results obtained in other glia or heterologous expression systems (Hoegg-Beiler et al., 2014). This indicates that additional factors are present in Bergmann glia, which keep ClC-2 closed under physiological conditions.

## 6.3 EAAT1/GLAST and EAAT2/GLT1 regulate intracellular chloride in Bergmann glia and allow dynamic adjustments during glutamatergic synaptic transmission

### 6.3.1 Glial EAAT anion channel function affects $[Cl^-]_{int}$

EAATs function as anion selective channels and as secondary active glutamate transporters. The deletion of the major EAAT in Bergmann glia, EAAT1/GLAST, leads to an increase in  $[Cl^-]_{int}$  (Fig. 5.9). Additional blocking experiments revealed that EAAT1/GLAST and EAAT2/GLT1 affect  $[Cl^-]_{int}$ . Blocking as well as deletion of these proteins affect both the transporting and anion channelling function. However, the obtained results can be explained by assuming that blocking or activation of EAAT results in changes in the chloride conductance, hence, altering the  $[Cl^-]_{int}$ . Furthermore, it was shown that blocking glial EAATs leaves the  $[Na^+]_{int}$  in astrocytes unaffected (Karus et al., 2015, Langer and Rose, 2009). The same was observed by Niklas J. Gerkau and Christine R. Rose, Institute for Neuroscience, Düsseldorf (Untiet et al., 2016) in Bergmann glia, thus changes in  $[Cl^-]_{int}$  are not due to a disruption of the glial sodium gradient. Glial EAATs have been described to be efficient glutamate transporters with small macroscopic anion currents, albeit studies from Niels Christian Danbolt revealed a very high amount of this protein (1.8 mg per g brain tissue) in the cerebellum (Lehre and Danbolt, 1998). Even if the anion current of every channel rather small, in total, the global deletion results in a significant increase of  $[Cl^-]_{int}$  of Bergmann glia, as shown here.

### 6.3.2 EAAT2/GLT1 appears not to be upregulated in *Slc1a3*<sup>-/-</sup> mice

Genetic ablation of EAAT1/GLAST and pharmacologically blocking of EAAT1/GLAST using the subtype specific blocker UCPH-101, showed a significant difference in the  $[Cl^-]_{int}$ . The increase in the  $[Cl^-]_{int}$  upon UCPH-101 application, above *Slc1a3*<sup>-/-</sup> levels indicated an upregulation of the expression of EAAT2/GLT1. A relative quantification of the expression levels did show a higher expression level for EAAT2/GLT1 in the EAAT1/GLAST *knock-out* animals, however, this difference is not significant (Fig. 5.10). Thus, EAAT2/GLT1 appears not to be upregulated in *Slc1a3*<sup>-/-</sup>. To further investigate this contradiction another method to quantify the exact amount of protein should be applied. The most exact information can be obtained by counting single proteins using electron microscopy as performed earlier in wild type (Lehre and Danbolt, 1998).

### 6.3.3 EAAT1/GLAST and EAAT2/GLT1 determine the $[Cl^-]_{int}$ during cerebellar maturation

The glial EAATs, EAAT1/GLAST and EAAT2/GLT1, not only contribute to set the  $[Cl^-]_{int}$ , but also mediate a developmental glial chloride switch (Fig. 5.12). Within the second postnatal week, the  $[Cl^-]_{int}$  in Bergmann glia drops from 50 to 34 mM. A similar decrease with a later onset ( $P > 9$ ) and a significant higher adult value of 41 mM could be observed in *Slc1a3*  $-/-$ . This glial chloride switch correlates with the upregulation of EAAT1/GLAST and EAAT2/GLT1 expression in the cerebellum (Holmseth et al., 2012, Ullensvang et al., 1997, Regan et al., 2007). The high  $[Cl^-]_{int}$  at early developmental stages may support dynamic volume adjustments during cell migration by allowing effective chloride effluxes through volume activated anion channels and via activation of KCC1 and KCC3 (Kahle et al., 2010). It is in this time period that Bergmann glia migrate together with Purkinje neurons from the ventricular zone towards the cortex (Yuasa, 1996). At the end of the first postnatal week (P7) these migrations are finalized and Bergmann glia sheath Purkinje neurons, which start the outgrowth of their dendritic trees (Yamada and Watanabe, 2002). At the same time, during the first postnatal week, Bergmann glia guide the way of granule cells along their fibres from the outer granule layer to the inner granule layer (Xu et al., 2013, Rakic, 1971). Thus, volume adjustments may support the migratory processes, which last until the end of the second postnatal week (Buffo and Rossi, 2013), when the  $[Cl^-]_{int}$  of Bergmann glia decreased to the adult value. Furthermore, Bergmann glia mediate GABA uptake by GABA transporters (GAT1, GAT3) from the extracellular space (Zhou and Danbolt, 2013). These transporters couple GABA uptake to sodium and chloride gradients and their function depends on the electrical gradient. Thus, changes in the  $[Cl^-]_{int}$  can lead to a modification of the GABA transport rates. While it is impossible to predict GABA transport rates from the  $[Cl^-]_{int}$ , it is possible to calculate the minimum  $[GABA]_{ext}$  of the thermodynamic equilibrium of this transport process with the following equation (8):

$$[GABA]_{out} = \frac{[Na^+]_{in}^2 [Cl^-]_{in} [GABA]_{in}}{[Na^+]_{out}^2 [Cl^-]_{out}} e^{\frac{UF}{RT}} \quad (8)$$

Using standard internal and external sodium and GABA concentrations, with  $[Na^+]_{int}$  of 14.6 mM and  $[GABA]_{int}$  of 2.3 mM, respectively (Zomot et al., 2007, Lee et al., 2011, Rose and Ransom, 1996), the  $[GABA]_{ext}$  at equilibrium results in 0.21  $\mu$ M in adult WT animals. During

cerebellar maturation, considering the glial chloride switch from 52 to 34 mM, the  $[GABA]_{ext}$  is predicted to change from 0.34 to 0.21  $\mu$ M. These developmental changes can contribute to neuronal migration, since immature neurons exhibit tonic GABAergic currents that modulates their movement (Demarque et al., 2002), and terminates at P15.

Furthermore, external GABA concentrations have been reported to affect cell migration (Luhmann et al., 2015). During cerebellar maturation Bergmann glia and granule cells are tightly connected, since Bergmann glia guide the granule cells through the molecular layer (Yamada and Watanabe, 2002). In the adult cerebellum Bergmann glia are functional closely connected to neurons (Grosche et al., 1999), and changes in extracellular GABA levels could affect inhibitory synaptic transmission. Furthermore, changes in  $[Cl^-]_{int}$  may affects GABA<sub>A</sub>-receptor mediated currents. As it was described before, that those currents are detectable in Bergmann glia of young animals while they are decreasing with age (Muller et al., 1994).

#### **6.3.4 The glial chloride switch in cerebellar Bergmann glia**

In neurons the upregulation of KCC2 during the first postnatal week decreases chloride and permits neuronal inhibition by opening ligand-gated channels via GABA or glycine release at mature inhibitory synapses (Rivera et al., 1999, Ganguly et al., 2001). This neuronal chloride switch occurs between postnatal day 5 and 14, with different timing for different parts of the brain (Delpire, 2000). No developmental alterations or changes in glial chloride concentrations have been reported before. In this work the glial chloride switch in Bergmann glia was newly-discovered (chapter 5.2.4), which occurs at the same time as the neuronal chloride switch. The glial chloride switch will possibly improve the GABAergic synaptic transmission by increasing glial GABA uptake rates due to decreasing the  $[Cl^-]_{int}$  and providing better signal to noise ratios in synaptic transmission.

#### **6.3.5 Dynamic adjustment of $[Cl^-]_{int}$ performed via glial EAATs during excitatory synaptic transmission**

Substrate application as well as measurements after electrical stimulation demonstrated a functional coupling of extracellular glutamate and a decreased  $[Cl^-]_{int}$ . Purkinje neurons receive input from parallel fibres via glutamatergic signals. This activation of EAAT anion channels causes a decrease of the  $[Cl^-]_{int}$ . Perfusion with Bicuculline during the electrical

stimulation lead to the same decrease in  $[Cl^-]_{int}$ , indicating, that these changes are not due to GABA<sub>A</sub> receptor opening.

The decrease of the  $[Cl^-]_{int}$  determined in wild type upon electrical stimulation results in predicted changes of  $[GABA]_{ext}$  down to 0.15  $\mu$ M. With this loop, glutamatergic synaptic transmission directly affects tonic inhibitory GABA currents in the cerebellar cortex. Purkinje neurons and granule cells express GABA<sub>A</sub> receptors with an EC<sub>50</sub> of 0.27  $\mu$ M (Saxena and Macdonald, 1996). Under physiological conditions these receptors show a high open probability and provide tonic GABAergic currents (Brickley et al., 1996). This crosstalk between inhibitory and excitatory synaptic transmissions depends on a damageable equilibrium. During pathological processes as upon neuronal cell death or during brain ischemia, increased extracellular glutamate concentrations will activate EAAT anion channels and decrease the  $[Cl^-]_{int}$  in glial cells, to values even below determined values during electrical stimulation measurements or substrate application. This change in the  $[Cl^-]_{int}$  can then reinforce the GABA uptake and reduce inhibitory synaptic transmission, and finally promote glutamate excitotoxicity and neuronal cell death (Danbolt, 2001). A model for this scenario is the gain of function mutation in EAAT1/GLAST, P290R. The increase in anion conductance mimics the permanently activated EAAT1/GLAST anion channel, this can lead to changes in the  $[Cl^-]_{int}$  followed by a modified neurotransmitter homeostasis and eventually may result in ataxia and epilepsy. The inverse process of a lost EAAT anion conductance appears less severe, as the milder phenotype of the *Slc1a3*<sup>-/-</sup> demonstrates. Nevertheless, it shows a slight motor incoordination, without increased mortality (Watase et al., 1998). EAAT1/GLAST is predominantly expressed in the cerebellum, a part of the brain which is not crucial for mammal's survival. This can be the difference compared to the glial EAAT2/GLT1 *knock-out* (*Slc1a2*<sup>-/-</sup>) mouse, since EAAT2/GLT1 is expressed in nearly every brain region. In the glial *knock-out* model no significant changes in extracellular glutamate levels were observed, thus it needs to be evaluated if this is due to an unsuitable method to measure glutamate uptake, as the authors discuss or if the missing anion channel plays a major role in the pathomechanism. A global *knock-out* of all EAAT2/GLT1 will heavily change the equilibrium due to the missing anion channel and can have a severe impact on the individual.

## 7 Conclusion

Glial excitatory amino acid transporters are described as efficient glutamate transporters with small macroscopic anion currents (Wadiche et al., 1995a), accordingly, it was shown that these proteins provide the major glutamate uptake, but the physiological role of their anion channel function remained completely unclear. My thesis identified, for the first time, a cellular role for the anion channel function of EAAT1/GLAST and EAAT2/GLT1 in glial cells. These EAAT anion channels are the central player in setting the  $[Cl^-]_{int}$  in Bergmann glia during cerebellar maturation and they dynamically adjust the  $[Cl^-]_{int}$  during neuronal synaptic transmission. Synaptically released glutamate increases the open probability of glial EAATs and decreases the  $[Cl^-]_{int}$ , which then stimulates the GABA uptake. During maturation the upregulation of EAAT1/GLAST and EAAT2/GLT1 expression leads to a glial chloride switch, which terminates neuronal migration by decreased  $[GABA]_{ext}$  via decreasing  $[Cl^-]_{int}$ . This glial chloride switch furthermore appears at the same time as the neuronal chloride switch and is likely to further improve inhibitory synaptic transmission. The data retrieved during my thesis reveals for the first time a crucial role of glial EAAT anion channels in brain function, reasoning that functional changes, such as in the gain of function mutation P290R, can lead to severe symptoms as ataxia and epilepsy. Furthermore, these findings provide the basic knowledge that will lead to new therapeutic approaches to treat these symptoms.

## 8 References

- ABDULLAEV, I. F., RUDKOUSKAYA, A., SCHOOLS, G. P., KIMELBERG, H. K. & MONGIN, A. A. 2006. Pharmacological comparison of swelling-activated excitatory amino acid release and Cl<sup>-</sup> currents in cultured rat astrocytes. *J Physiol*, 572, 677-689.
- ABRAHAMSEN, B., SCHNEIDER, N., ERICHSEN, M. N., HUYNH, T. H., FAHLKE, Ch., BUNCH, L. & JENSEN, A. A. 2013. Allosteric modulation of an excitatory amino acid transporter: the subtype-selective inhibitor UCPH-101 exerts sustained inhibition of EAAT1 through an intramonomeric site in the trimerization domain. *J Neurosci*, 33, 1068-1087.
- BECKER, W. 2005. *Advanced time-correlated single photon counting techniques*, Springer Series in Chemical Physics 81: (doi: 10.1007/3-540-28882-1).
- BEKAR, L. K. & WALZ, W. 2002. Intracellular chloride modulates A-type potassium currents in astrocytes. *Glia*, 39, 207-216.
- BENNAY, M., LANGER, J., MEIER, S. D., KAFITZ, K. W. & ROSE, C. R. 2008. Sodium signals in cerebellar Purkinje neurons and Bergmann glial cells evoked by glutamatergic synaptic transmission. *Glia*, 56, 1138-1149.
- BERGLES, D. E., DZUBAY, J. A. & JAHR, C. E. 1997. Glutamate transporter currents in bergmann glial cells follow the time course of extrasynaptic glutamate. *Proc Natl Acad Sci U S A*, 94, 14821-14825.
- BLANZ, J., SCHWEIZER, M., AUBERSON, M., MAIER, H., MUENSCHER, A., HUBNER, C. A. & JENTSCH, T. J. 2007. Leukoencephalopathy upon disruption of the chloride channel CIC-2. *Journal of Neuroscience*, 27, 6581-6589.
- BOSL, M. R., STEIN, V., HUBNER, C., ZDEBIK, A. A., JORDT, S. E., MUKHOPADHYAY, A. K., DAVIDOFF, M. S., HOLSTEIN, A. F. & JENTSCH, T. J. 2001. Male germ cells and photoreceptors, both dependent on close cell-cell interactions, degenerate upon CIC-2 Cl<sup>-</sup> channel disruption. *EMBO J*, 20, 1289-1299.
- BRAITENBERG, V. & ATWOOD, R. P. 1958. Morphological observations on the cerebellar cortex. *J Comp Neurol*, 109, 1-33.
- BRICKLEY, S. G., CULL-CANDY, S. G. & FARRANT, M. 1996. Development of a tonic form of synaptic inhibition in rat cerebellar granule cells resulting from persistent activation of GABA<sub>A</sub> receptors. *J Physiol*, 497 (Pt 3), 753-759.
- BUFFO, A. & ROSSI, F. 2013. Origin, lineage and function of cerebellar glia. *Prog Neurobiol*, 109, 42-63.
- CAHOY, J. D., EMERY, B., KAUSHAL, A., FOO, L. C., ZAMANIAN, J. L., CHRISTOPHERSON, K. S., XING, Y., LUBISCHER, J. L., KRIEG, P. A., KRUPENKO, S. A., THOMPSON, W. J. & BARRES, B. A. 2008.

- A transcriptome database for astrocytes, neurons, and oligodendrocytes: a new resource for understanding brain development and function. *J Neurosci*, 28, 264-278.
- CHAUDHRY, F. A., LEHRE, K. P., VAN LOOKEREN CAMPAGNE, M., OTTERSEN, O. P., DANBOLT, N. C. & STORM-MATHISEN, J. 1995. Glutamate transporters in glial plasma membranes: highly differentiated localizations revealed by quantitative ultrastructural immunocytochemistry. *Neuron*, 15, 711-720.
- CLARK, B. A. & BARBOUR, B. 1997. Currents evoked in Bergmann glial cells by parallel fibre stimulation in rat cerebellar slices. *J Physiol*, 502 (Pt 2), 335-350.
- CURTIS, D. R., DUGGAN, A. W., FELIX, D. & JOHNSTON, G. A. 1971. Bicuculline, an antagonist of GABA and synaptic inhibition in the spinal cord of the cat. *Brain Res*, 32, 69-96.
- DANBOLT, N. C. 2001. Glutamate uptake. *Prog Neurobiol*, 65, 1-105.
- DEHNES, Y., CHAUDHRY, F. A., ULLENSVANG, K., LEHRE, K. P., STORM-MATHISEN, J. & DANBOLT, N. C. 1998. The glutamate transporter EAAT4 in rat cerebellar Purkinje cells: a glutamate-gated chloride channel concentrated near the synapse in parts of the dendritic membrane facing astroglia. *J Neurosci*, 18, 3606-3619.
- DELPIRE, E. 2000. Cation-chloride cotransporters in neuronal communication. *News Physiol Sci*, 15, 309-312.
- DEMARQUE, M., REPRESA, A., BECQ, H., KHALILOV, I., BEN-ARI, Y. & ANIKSZTEJN, L. 2002. Paracrine intercellular communication by a Ca<sup>2+</sup>- and SNARE-independent release of GABA and glutamate prior to synapse formation. *Neuron*, 36, 1051-1061.
- DOYLE, J. P., DOUGHERTY, J. D., HEIMAN, M., SCHMIDT, E. F., STEVENS, T. R., MA, G., BUPP, S., SHRESTHA, P., SHAH, R. D., DOUGHTY, M. L., GONG, S., GREENGARD, P. & HEINTZ, N. 2008. Application of a translational profiling approach for the comparative analysis of CNS cell types. *Cell*, 135, 749-762.
- EDWARDS, F. A., KONNERTH, A., SAKMANN, B. & TAKAHASHI, T. 1989. A thin slice preparation for patch clamp recordings from neurones of the mammalian central nervous system. *Pflugers Arch*, 414, 600-612.
- FAIRMAN, W. A., VANDENBERG, R. J., ARRIZA, J. L., KAVANAUGH, M. P. & AMARA, S. G. 1995. An excitatory amino-acid transporter with properties of a ligand-gated chloride channel. *Nature*, 375, 599-603.
- FOO, L. C., ALLEN, N. J., BUSHONG, E. A., VENTURA, P. B., CHUNG, W. S., ZHOU, L., CAHOY, J. D., DANEMAN, R., ZONG, H., ELLISMAN, M. H. & BARRES, B. A. 2011. Development of a method for the purification and culture of rodent astrocytes. *Neuron*, 71, 799-811.
- GANGULY, K., SCHINDER, A. F., WONG, S. T. & POO, M. 2001. GABA itself promotes the developmental switch of neuronal GABAergic responses from excitation to inhibition. *Cell*, 105, 521-532.

- GEIGER, A., RUSSO, L., GENSCHE, T., THESTRUP, T., BECKER, S., HOPFNER, K. P., GRIESINGER, C., WITTE, G. & GRIESBECK, O. 2012. Correlating calcium binding, Forster resonance energy transfer, and conformational change in the biosensor TN-XXL. *Biophys J*, 102, 2401-2410.
- GENSCH, T., UNTIET, V., FRANZEN, A., KOVERMANN, P. & FAHLKE, Ch. 2015. Determination of Intracellular Chloride Concentrations by Fluorescence Lifetime Imaging. *Advanced Time-Correlated Single Photon Counting Applications*. Springer Series in Chemical Physics 111, 189-211.
- GILBERT, D., FRANJIC-WURTZ, C., FUNK, K., GENSCHE, T., FRINGS, S. & MOHRLEN, F. 2007. Differential maturation of chloride homeostasis in primary afferent neurons of the somatosensory system. *Int J Dev Neurosci*, 25, 479-489.
- GLICKSTEIN, M., STRATA, P. & VOOGD, J. 2009. Cerebellum: history. *Neuroscience*, 162, 549-559.
- GLICKSTEIN, M., SULTAN, F. & VOOGD, J. 2011. Functional localization in the cerebellum. *Cortex*, 47, 59-80.
- GREWER, C., GAMEIRO, A. & RAUEN, T. 2014. SLC1 glutamate transporters. *Pflugers Arch*, 466, 3-24.
- GROSCHKE, J., MATYASH, V., MOLLER, T., VERKHRATSKY, A., REICHENBACH, A. & KETTENMANN, H. 1999. Microdomains for neuron-glia interaction: parallel fiber signaling to Bergmann glial cells. *Nat Neurosci*, 2, 139-143.
- HABELA, C. W., ERNEST, N. J., SWINDALL, A. F. & SONTHEIMER, H. 2009. Chloride accumulation drives volume dynamics underlying cell proliferation and migration. *J Neurophysiol*, 101, 750-757.
- HOEGG-BEILER, M. B., SIRISI, S., OROZCO, I. J., FERRER, I., HOHENSEE, S., AUBERSON, M., GODDE, K., VILCHES, C., DE HEREDIA, M. L., NUNES, V., ESTEVEZ, R. & JENTSCH, T. J. 2014. Disrupting MLC1 and GlialCAM and CIC-2 interactions in leukodystrophy entails glial chloride channel dysfunction. *Nat Commun*, 5, 3475.
- HOLMSETH, S., DEHNES, Y., HUANG, Y. H., FOLLIN-ARBELET, V. V., GRUTLE, N. J., MYLONAKOU, M. N., PLACHEZ, C., ZHOU, Y., FURNESS, D. N., BERGLES, D. E., LEHRE, K. P. & DANBOLT, N. C. 2012. The density of EAAC1 (EAAT3) glutamate transporters expressed by neurons in the mammalian CNS. *J Neurosci*, 32, 6000-6013.
- HUBNER, C. A., LORKE, D. E. & HERMANS-BORGMEYER, I. 2001. Expression of the Na-K-2Cl<sup>-</sup> cotransporter NKCC1 during mouse development. *Mech Dev*, 102, 267-269.
- HYZINSKI-GARCIA, M. C., RUDKOUSKAYA, A. & MONGIN, A. A. 2014. LRRC8A protein is indispensable for swelling-activated and ATP-induced release of excitatory amino acids in rat astrocytes. *J Physiol*, 592, 4855-4862.
- ITO, M., YOSHIDA, M., OBATA, K., KAWAI, N. & UDO, M. 1970. Inhibitory control of intracerebellar nuclei by the purkinje cell axons. *Exp Brain Res*, 10, 64-80.

- JEN, J. C., GRAVES, T. D., HESS, E. J., HANNA, M. G., GRIGGS, R. C., BALOH, R. W. & INVESTIGATORS, C. 2007. Primary episodic ataxias: diagnosis, pathogenesis and treatment. *Brain*, 130, 2484-2493.
- JEN, J. C., WAN, J., PALOS, T. P., HOWARD, B. D. & BALOH, R. W. 2005. Mutation in the glutamate transporter EAAT1 causes episodic ataxia, hemiplegia, and seizures. *Neurology*, 65, 529-534.
- JORDT, S. E. & JENTSCH, T. J. 1997. Molecular dissection of gating in the ClC-2 chloride channel. *EMBO J*, 16, 1582-1592.
- JUNGBLUT, M., TIVERON, M. C., BARRAL, S., ABRAHAMSEN, B., KNOBEL, S., PENNARTZ, S., SCHMITZ, J., PERRAUT, M., PFRIEGER, F. W., STOFFEL, W., CREMER, H. & BOSIO, A. 2012. Isolation and characterization of living primary astroglial cells using the new GLAST-specific monoclonal antibody ACSA-1. *Glia*, 60, 894-907.
- KAHLE, K. T., RINEHART, J. & LIFTON, R. P. 2010. Phosphoregulation of the Na-K-2Cl and K-Cl cotransporters by the WNK kinases. *Biochim Biophys Acta*, 1802, 1150-1158.
- KANAKA, C., OHNO, K., OKABE, A., KURIYAMA, K., ITOH, T., FUKUDA, A. & SATO, K. 2001. The differential expression patterns of messenger RNAs encoding K-Cl cotransporters (KCC1,2) and Na-K-2Cl cotransporter (NKCC1) in the rat nervous system. *Neuroscience*, 104, 933-946.
- KANEKO, H., PUTZIER, I., FRINGS, S., KAUPP, U. B. & GENSCHE, T. 2004. Chloride accumulation in mammalian olfactory sensory neurons. *J Neurosci*, 24, 7931-7938.
- KARUS, C., MONDRAGAO, M. A., ZIEMENS, D. & ROSE, C. R. 2015. Astrocytes restrict discharge duration and neuronal sodium loads during recurrent network activity. *Glia*, 63, 936-957.
- KELLY, T., KAFITZ, K. W., RODERIGO, C. & ROSE, C. R. 2009. Ammonium-evoked alterations in intracellular sodium and pH reduce glial glutamate transport activity. *Glia*, 57, 921-934.
- KETTENMANN, H., BACKUS, K. H. & SCHACHNER, M. 1987.  $\gamma$ -Aminobutyric acid opens Cl<sup>-</sup> channels in cultured astrocytes. *Brain Res*, 404, 1-9.
- KIMELBERG, H. K. 1981. Active accumulation and exchange transport of chloride in astroglial cells in culture. *Biochim Biophys Acta*, 646, 179-184.
- KIMELBERG, H. K., BIDDLECOME, S. & BOURKE, R. S. 1979. SITS-inhibitable Cl<sup>-</sup> transport and Na<sup>+</sup>-dependent H<sup>+</sup> production in primary astroglial cultures. *Brain Res*, 173, 111-124.
- KOMURO, H., YACUBOVA, E., YACUBOVA, E. & RAKIC, P. 2001. Mode and tempo of tangential cell migration in the cerebellar external granular layer. *J Neurosci*, 21, 527-540.
- KOVALCHUK, Y. & GARASCHUK, O. 2012. Two-photon chloride imaging using MQAE in vitro and in vivo. *Cold Spring Harb Protoc*, 2012, 778-785.
- KRAPF, R., BERRY, C. A. & VERKMAN, A. S. 1988. Estimation of intracellular chloride activity in isolated perfused rabbit proximal convoluted tubules using a fluorescent indicator. *Biophys J*, 53, 955-962.

- LANGER, J. & ROSE, C. R. 2009. Synaptically induced sodium signals in hippocampal astrocytes in situ. *J Physiol*, 587, 5859-5877.
- LEE, A., ANDERSON, A. R., STEVENS, M., BEASLEY, S., BARNETT, N. L. & POW, D. V. 2013. Excitatory amino acid transporter 5 is widely expressed in peripheral tissues. *Eur J Histochem*, 57, e11.
- LEE, M., MCGEER, E. G. & MCGEER, P. L. 2011. Mechanisms of GABA release from human astrocytes. *Glia*, 59, 1600-1611.
- LEHRE, K. P. & DANBOLT, N. C. 1998. The number of glutamate transporter subtype molecules at glutamatergic synapses: chemical and stereological quantification in young adult rat brain. *J Neurosci*, 18, 8751-8757.
- LEVY, L. M., WARR, O. & ATTWELL, D. 1998. Stoichiometry of the glial glutamate transporter GLT-1 expressed inducibly in a Chinese hamster ovary cell line selected for low endogenous Na<sup>+</sup>-dependent glutamate uptake. *J Neurosci*, 18, 9620-9628.
- LUHMANN, H. J., FUKUDA, A. & KILB, W. 2015. Control of cortical neuronal migration by glutamate and GABA. *Front Cell Neurosci*, 9, 4.
- MACHTENS, J. P., KORTZAK, D., LANSCHKE, C., LEINENWEBER, A., KILIAN, P., BEGEMANN, B., ZACHARIAE, U., EWERS, D., DE GROOT, B. L., BRIONES, R. & FAHLKE, Ch. 2015. Mechanisms of anion conduction by coupled glutamate transporters. *Cell*, 160, 542-553.
- MACVICAR, B. A., TSE, F. W., CRICHTON, S. A. & KETTENMANN, H. 1989. GABA-activated Cl<sup>-</sup> channels in astrocytes of hippocampal slices. *J Neurosci*, 9, 3577-3583.
- MARANDI, N., KONNERTH, A. & GARASCHUK, O. 2002. Two-photon chloride imaging in neurons of brain slices. *Pflugers Arch*, 445, 357-365.
- MEIER, S. D., KOVALCHUK, Y. & ROSE, C. R. 2006. Properties of the new fluorescent Na<sup>+</sup> indicator CoroNa Green: comparison with SBFI and confocal Na<sup>+</sup> imaging. *J Neurosci Methods*, 155, 251-259.
- MERCADO, A., SONG, L., VAZQUEZ, N., MOUNT, D. B. & GAMBA, G. 2000. Functional comparison of the K<sup>+</sup>-Cl<sup>-</sup> cotransporters KCC1 and KCC4. *J Biol Chem*, 275, 30326-30334.
- MIKAWA, S., WANG, C., SHU, F., WANG, T., FUKUDA, A. & SATO, K. 2002. Developmental changes in KCC1, KCC2 and NKCC1 mRNAs in the rat cerebellum. *Brain Res Dev Brain Res*, 136, 93-100.
- MIM, C., BALANI, P., RAUEN, T. & GREWER, C. 2005. The glutamate transporter subtypes EAAT4 and EAATs 1-3 transport glutamate with dramatically different kinetics and voltage dependence but share a common uptake mechanism. *J Gen Physiol*, 126, 571-589.
- MOUNT, D. B., MERCADO, A., SONG, L., XU, J., GEORGE, A. L., JR., DELPIRE, E. & GAMBA, G. 1999. Cloning and characterization of KCC3 and KCC4, new members of the cation-chloride cotransporter gene family. *J Biol Chem*, 274, 16355-16362.

- MULLER, T., FRITSCHY, J. M., GROSCHE, J., PRATT, G. D., MOHLER, H. & KETTENMANN, H. 1994. Developmental regulation of voltage-gated K<sup>+</sup> channel and GABA<sub>A</sub> receptor expression in Bergmann glial cells. *J Neurosci*, 14, 2503-2514.
- NOBILE, M., PUSCH, M., RAPISARDA, C. & FERRONI, S. 2000. Single-channel analysis of a ClC-2-like chloride conductance in cultured rat cortical astrocytes. *FEBS Lett*, 479, 10-14.
- PAYNE, J. A., RIVERA, C., VOIPIO, J. & KAILA, K. 2003. Cation-chloride co-transporters in neuronal communication, development and trauma. *Trends Neurosci*, 26, 199-206.
- PETR, G. T., SUN, Y., FREDERICK, N. M., ZHOU, Y., DHAMNE, S. C., HAMEED, M. Q., MIRANDA, C., BEDOYA, E. A., FISCHER, K. D., ARMSEN, W., WANG, J., DANBOLT, N. C., ROTENBERG, A., AOKI, C. J. & ROSENBERG, P. A. 2015. Conditional deletion of the glutamate transporter GLT-1 reveals that astrocytic GLT-1 protects against fatal epilepsy while neuronal GLT-1 contributes significantly to glutamate uptake into synaptosomes. *J Neurosci*, 35, 5187-5201.
- RAKIC, P. 1971. Neuron-glia relationship during granule cell migration in developing cerebellar cortex. A Golgi and electronmicroscopic study in Macacus Rhesus. *J Comp Neurol*, 141, 283-312.
- REGAN, M. R., HUANG, Y. H., KIM, Y. S., DYKES-HOBERG, M. I., JIN, L., WATKINS, A. M., BERGLES, D. E. & ROTHSTEIN, J. D. 2007. Variations in promoter activity reveal a differential expression and physiology of glutamate transporters by glia in the developing and mature CNS. *J Neurosci*, 27, 6607-6619.
- RIVERA, C., VOIPIO, J., PAYNE, J. A., RUUSUVUORI, E., LAHTINEN, H., LAMSA, K., PIRVOLA, U., SAARMA, M. & KAILA, K. 1999. The K<sup>+</sup>/Cl<sup>-</sup> co-transporter KCC2 renders GABA hyperpolarizing during neuronal maturation. *Nature*, 397, 251-255.
- ROSE, C. R. & RANSOM, B. R. 1996. Intracellular sodium homeostasis in rat hippocampal astrocytes. *Journal of Physiology-London*, 491, 291-305.
- SAXENA, N. C. & MACDONALD, R. L. 1996. Properties of putative cerebellar  $\gamma$ -aminobutyric acid<sub>A</sub> receptor isoforms. *Mol Pharmacol*, 49, 567-579.
- SCHMITT, A., ASAN, E., PUSCHEL, B., JONS, T. & KUGLER, P. 1996. Expression of the glutamate transporter GLT1 in neural cells of the rat central nervous system: non-radioactive in situ hybridization and comparative immunocytochemistry. *Neuroscience*, 71, 989-1004.
- SCHREINER, A. E., DURRY, S., AIDA, T., STOCK, M. C., RUTHER, U., TANAKA, K., ROSE, C. R. & KAFITZ, K. W. 2014. Laminar and subcellular heterogeneity of GLAST and GLT-1 immunoreactivity in the developing postnatal mouse hippocampus. *J Comp Neurol*, 522, 204-224.
- SCHWAB, A., FABIAN, A., HANLEY, P. J. & STOCK, C. 2012. Role of ion channels and transporters in cell migration. *Physiol Rev*, 92, 1865-1913.

- SHIMAMOTO, K., LEBRUN, B., YASUDA-KAMATANI, Y., SAKAITANI, M., SHIGERI, Y., YUMOTO, N. & NAKAJIMA, T. 1998. DL-threo- $\beta$ -benzyloxyaspartate, a potent blocker of excitatory amino acid transporters. *Mol Pharmacol*, 53, 195-201.
- SHINODA, Y., SUGIHARA, I., WU, H. S. & SUGIUCHI, Y. 2000. The entire trajectory of single climbing and mossy fibers in the cerebellar nuclei and cortex. *Prog Brain Res*, 124, 173-186.
- SIK, A., SMITH, R. L. & FREUND, T. F. 2000. Distribution of chloride channel-2-immunoreactive neuronal and astrocytic processes in the hippocampus. *Neuroscience*, 101, 51-65.
- STALEY, K., SMITH, R., SCHAACK, J., WILCOX, C. & JENTSCH, T. J. 1996. Alteration of GABA<sub>A</sub> receptor function following gene transfer of the CLC-2 chloride channel. *Neuron*, 17, 543-551.
- STORCK, T., SCHULTE, S., HOFMANN, K. & STOFFEL, W. 1992. Structure, expression, and functional analysis of a Na<sup>+</sup>-dependent glutamate/aspartate transporter from rat brain. *Proc Natl Acad Sci U S A*, 89, 10955-10959.
- SU, G., KINTNER, D. B. & SUN, D. D. 2002. Contribution of Na<sup>+</sup>-K<sup>+</sup>-Cl<sup>-</sup> cotransporter to high-[K<sup>+</sup>]<sub>o</sub>-induced swelling and EAA release in astrocytes. *American Journal of Physiology-Cell Physiology*, 282, C1136-C1146.
- SULTAN, F. 2014. From cerebellar texture to movement optimization. *Biol Cybern.*  
Doi:10.1007/s00422-014-0618-2
- TANAKA, K., WATASE, K., MANABE, T., YAMADA, K., WATANABE, M., TAKAHASHI, K., IWAMA, H., NISHIKAWA, T., ICHIHARA, N., KIKUCHI, T., OKUYAMA, S., KAWASHIMA, N., HORI, S., TAKIMOTO, M. & WADA, K. 1997. Epilepsy and exacerbation of brain injury in mice lacking the glutamate transporter GLT-1. *Science*, 276, 1699-1702.
- TANAKA, M., YAMAGUCHI, K., TATSUKAWA, T., THEIS, M., WILLECKE, K. & ITOHARA, S. 2008. Connexin43 and bergmann glial gap junctions in cerebellar function. *Front Neurosci*, 2, 225-233.
- TZINGOUNIS, A. V. & WADICHE, J. I. 2007. Glutamate transporters: confining runaway excitation by shaping synaptic transmission. *Nat Rev Neurosci*, 8, 935-947.
- ULLENSVANG, K., LEHRE, K. P., STORM-MATHISEN, J. & DANBOLT, N. C. 1997. Differential developmental expression of the two rat brain glutamate transporter proteins GLAST and GLT. *Eur J Neurosci*, 9, 1646-1655.
- UNTIET, V., KOVERMANN, P., GERKAU, N. J., GENSCHE, T., ROSE, C. R., & FAHLKE, Ch. 2016. Glutamate transporter-associated anion channels adjust intracellular chloride concentrations during glial maturation. *Glia*, in press.
- VAN BEUGEN, B. J., GAO, Z., BOELE, H. J., HOEBEEK, F. & DE ZEEUW, C. I. 2013. High frequency burst firing of granule cells ensures transmission at the parallel fiber to purkinje cell synapse at the cost of temporal coding. *Front Neural Circuits*, 7, 95.

- VERKMAN, A. S., SELLERS, M. C., CHAO, A. C., LEUNG, T. & KETCHAM, R. 1989. Synthesis and characterization of improved chloride-sensitive fluorescent indicators for biological applications. *Anal Biochem*, 178, 355-361.
- VERUKI, M. L., MORKVE, S. H. & HARTVEIT, E. 2006. Activation of a presynaptic glutamate transporter regulates synaptic transmission through electrical signaling. *Nat Neurosci*, 9, 1388-1396.
- VOUTSINOS-PORCHE, B., KNOTT, G., TANAKA, K., QUAIRIAUX, C., WELKER, E. & BONVENTO, G. 2003. Glial glutamate transporters and maturation of the mouse somatosensory cortex. *Cereb Cortex*, 13, 1110-1121.
- WADICHE, J. I., AMARA, S. G. & KAVANAUGH, M. P. 1995a. Ion Fluxes Associated with Excitatory Amino-Acid-Transport. *Neuron*, 15, 721-728.
- WADICHE, J. I., AMARA, S. G. & KAVANAUGH, M. P. 1995b. Ion fluxes associated with excitatory amino acid transport. *Neuron*, 15, 721-728.
- WALZ, W. & HERTZ, L. 1983. Comparison between fluxes of potassium and of chloride in astrocytes in primary cultures. *Brain Res*, 277, 321-328.
- WATASE, K., HASHIMOTO, K., KANO, M., YAMADA, K., WATANABE, M., INOUE, Y., OKUYAMA, S., SAKAGAWA, T., OGAWA, S., KAWASHIMA, N., HORI, S., TAKIMOTO, M., WADA, K. & TANAKA, K. 1998. Motor discoordination and increased susceptibility to cerebellar injury in GLAST mutant mice. *European Journal of Neuroscience*, 10, 976-988.
- WERSINGER, E., SCHWAB, Y., SAHEL, J. A., RENDON, A., POW, D. V., PICAUD, S. & ROUX, M. J. 2006. The glutamate transporter EAAT5 works as a presynaptic receptor in mouse rod bipolar cells. *J Physiol*, 577, 221-234.
- WINTER, N., KOVERMANN, P. & FAHLKE, Ch. 2012. A point mutation associated with episodic ataxia 6 increases glutamate transporter anion currents. *Brain*, 135, 3416-3425.
- XU, H., YANG, Y., TANG, X., ZHAO, M., LIANG, F., XU, P., HOU, B., XING, Y., BAO, X. & FAN, X. 2013. Bergmann glia function in granule cell migration during cerebellum development. *Mol Neurobiol*, 47, 833-844.
- YAMADA, K. & WATANABE, M. 2002. Cytodifferentiation of Bergmann glia and its relationship with Purkinje cells. *Anat Sci Int*, 77, 94-108.
- YAN, Y., DEMPSEY, R. J. & SUN, D. 2001. Expression of Na<sup>+</sup>-K<sup>+</sup>-Cl<sup>-</sup> cotransporter in rat brain during development and its localization in mature astrocytes. *Brain Res*, 911, 43-55.
- YUASA, S. 1996. Bergmann glial development in the mouse cerebellum as revealed by tenascin expression. *Anat Embryol (Berl)*, 194, 223-234.
- ZERANGUE, N. & KAVANAUGH, M. P. 1996. Flux coupling in a neuronal glutamate transporter. *Nature*, 383, 634-637.

- ZHOU, Y. & DANBOLT, N. C. 2013. GABA and Glutamate Transporters in Brain. *Front Endocrinol (Lausanne)*, 4, 165.
- ZIFARELLI, G. & PUSCH, M. 2012. A kick-start for CLC antiporters' pharmacology. *Chem Biol*, 19, 1358-1359.
- ZOMOT, E., BENDAHAN, A., QUICK, M., ZHAO, Y., JAVITCH, J. A. & KANNER, B. I. 2007. Mechanism of chloride interaction with neurotransmitter:sodium symporters. *Nature*, 449, 726-730.

## 9 Manufacturers

**Abcam**, Cambridge, UK

**AppliChem**, Darmstadt, Germany

**Becker & Hickl**, Berlin, Germany

**BioRad**, München, Germany

**Chemicon**, Temecula, CA, USA

**Enzo**, Lörrach, Germany

**Eurofins Genomics**, Ebersberg, Germany

**GE Healthcare**, Solingen, Germany

**Life Technologies**, Darmstadt, Germany

**MACS Milteny Biotec**, Bergisch Gladbach, Germany

**Merck**, Darmstadt, Germany

**Molecular Devices LLC**, Sunnyvale, CA, USA

**Newport Spectra Physics**, Irvine, CA, USA

**Nikon Instruments Europe**, Amsterdam, the Netherlands

**Omega Optical**, Brattleboro, VT, USA

**Peqlab**, Erlangen, Germany

**Photon Technology International**, Birmingham, NJ, USA

**Picoquant**, Berlin, Germany

**Santa Cruz Biotechnology**, Heidelberg, Germany

**Science Products GmbH**, Hofheim, Germany

**Serva Electrophoresis**, Heidelberg, Germany

**Shimadzu Europa GmbH**, Duisburg, Germany

**Sigma-Aldrich**, Munich, Germany

**Syngene**, Cambridge, UK

**Thermo Fischer**, Darmstadt, Germany

**Thermo Scientific**, Braunschweig, Germany

**Tocris**, Bristol, UK

**Warner Instruments**, Hamden, CT, USA

## 10 Abbreviations

AB	Antibody
AM-ester	Aceto-methyl
BG	Bergmann glia
Bic	Bicuculline
bp	Base pairs
BSA	bovine serum albumin
CCC	Cation chloride cotransporter
CI	Confidence interval
Cl <sup>-</sup>	Chloride
[Cl <sup>-</sup> ] <sub>int</sub>	Intracellular chloride concentration
ClC	Chloride channel
CNS	Central nervous system
DCN	Deep cerebellar nucleus
DIV	Days in vitro
E	Energy
EA	Episodic ataxia
EAAT	Excitatory amino acid transporter
ES	Extracellular solution
FZJ	Forschungszentrum Jülich
GABA	Gamma amino isobutyric acid
GAT	GABA transporter
GC	Granule cell
<i>Clcn2</i> <sup>-/-</sup>	ClC-2 ( <i>Clcn2</i> ) knock-out
GLAST	Mammalian EAAT1
GLT1	Mammalian EAAT2
Gp	Guinea pig
<i>h</i>	Planck constant
HBEGF	Heparin binding epidermal growth factor
HRP	Horseradish peroxidase
IRF	Internal response function

IS	Intracellular solution
K <sup>+</sup>	Potassium
K <sub>f</sub>	Rate of spontaneous emission
K <sub>nr</sub>	Non-radiative decay
K <sub>q</sub>	Decay in dependence of quencher
K <sub>SV</sub>	Stern-Volmer constant
KCC	Potassium Chloride cotransporter
KO	Knock-out
λ	Wavelength
MQAE	1-(Ethoxycarbonylmethyl)-6-methoxyquinolinium bromide
ms	Mouse
Na <sup>+</sup>	Sodium
NKCC	Sodium Potassium Chloride Cotransporter
p	Level of significance
P	Postnatal day
P290R	Proline at position 290 substituted by arginine
PBS	Phosphate buffered saline
PC	Purkinje cell
PCR	Polymerase Chain Reaction
PF	Parallel fibre
R <sup>2</sup>	Determination coefficient
rb	Rabbit
RT	Room temperature
S <sub>0</sub>	Ground state
S <sub>1</sub>	Excited state
SD	Standard deviation
SDS	Sodium dodecyl sulfate
SLC	Solute carrier family
<i>Slc1a3</i> <sup>-/-</sup>	EAAT1/GLAST ( <i>Slc1a3</i> ) knock-out
<i>Slc1a2</i> <sup>-/-</sup>	EAAT2/GLT1 ( <i>Slc1a2</i> ) knock-out
SP	Short pass
Stimu	Stimulation

$\tau$	Fluorescence lifetime
TBS	Tris buffered saline
TCSPC	Time Correlated Single Photon Counting
$\nu$	Wave frequency
V	Volt
VRAC	Volume-regulated anion channel
VSOC	Volume-sensitive organic anion channel
WM	White matter
WT	Wild type



## **11 Eidesstattliche Versicherung**

Ich versichere an Eides Statt, dass die Dissertation von mir selbstständig und ohne unzulässige fremde Hilfe unter Beachtung der „Grundsätze zur Sicherung guter wissenschaftlicher Praxis an der Heinrich-Heine-Universität Düsseldorf“ erstellt worden ist.

Jülich, 15. Dezember 2015

---

Verena Untiet



## Danksagung

Im Folgenden möchte ich mich bei allen herzlich bedanken, die mich in den vergangenen Jahren unterstützt und zum Gelingen dieser Arbeit beigetragen haben.

Ich danke in erster Linie meinem Doktorvater Herrn Prof. Dr. Christoph Fahlke. Er hat mir nicht nur ermöglicht an diesem besonderen Forschungsprojekt in seinem Institut zu arbeiten, sondern er hat mich auch immer unterstützt und mich dazu ermuntert meine Daten sowohl auf nationaler, als auch auf internationaler Ebene vorzustellen.

Ebenfalls bedanke ich mich bei Frau Prof. Dr. Christine R. Rose, für die vielen guten Ratschläge und Ideen, wie auch für die Übernahme des Zweitgutachtens dieser Arbeit.

Des Weiteren möchte ich mich bei meinen beiden Betreuern, Thomas Gensch und Peter Kovermann, für ihr Engagement und die fortwährende Unterstützung bedanken.

Ich danke meinen lieben Kollegen Anita, Patty, Raul, Arne, Rudi, Jan-Philipp, Christoph, Nadine, Meike, sowie allen Mitarbeitern des ICS-4.

Besonderer Dank gilt meinen Eltern, sowie meiner Schwester und meiner gesamten Familie, die mich schon mein ganzes Leben uneingeschränkt unterstützt und damit den Grundstein für meine Laufbahn gelegt haben.

Für die persönliche Unterstützung in turbulenten Zeiten und für alle unvergesslichen Erlebnisse und schönen Momente auf der Arbeit und privat danke ich Felix, Anna, Rachel, Ike, Lena, Katha, Céline, Laura, Henny, Anne und Bastian.

Mein Dank gilt außerdem Laura Klotz für die Sprachkorrektur meiner Arbeit.